

INTERNSHIP DELTARES

Modeling particle drifters using a 3D velocity field and Stokes drift in the German Bight

S.C. Ruiter

supervised by
Prof. dr. ir. Martin Verlaan
Environmental Hydrodynamics and Forecasting
Deltares

June 5, 2020

Abstract

A Lagrangian particle model is studied in the German Bight, where the effect of using a 3D and a 2D water velocity model are reviewed. In this model, the Stokes drift is added to the particle velocity and estimated using the JONSWAP spectrum. Here, we found the 3D model to give better results compared to the 2D model and is capable in estimating the trajectories. Moreover, the inclusion of Stokes drift was not accurate enough to improve the results, neither in the 2D or 3D model. A better model for including wave effects should be explored to improve the particle model.

1 Introduction

Every year, more plastic is produced, and as a result more plastic waste. Unfortunately, large amounts of this end up in rivers and eventually in the ocean circulation. Since this plastic can be found in all parts of the ocean[1], a better understanding of the ocean circulation is required to pinpoint where this plastic litter will accumulate. Numerical models are an important tool in the development of this understanding.[2]

One of these models uses virtual particles and simulates their trajectories in the sea. In this study, this particle model is studied in the German Bight. In this region, Meyerjürgens et al.[3] employed floating drifters and measured their trajectories. This empirical data is important in the verification of the model.

In this study, the effect of using a 2D and 3D velocity field for the water current in this model is studied, in combination with the use of Stokes drift.

2 Background

In fluid dynamics, there are typically two ways of specifying a flow field, the Eulerian and Lagrangian specification. The Eulerian framework focuses on a fixed location in space, and describes the flow of a fluid over time at that location, whereas in the Lagrangian framework, a fluid parcel is tracked over time and describes the flow as it moves. In this particle model, the Lagrangian framework is used to track virtual floating particles in the German Bight over time. These Lagrangian particles represent fluid parcels or a small particles at the sea surface, such as plastic litter, and as such has a position on the sea. How these particles move over time, depends on the water and air near the particle, and described in detail in the next section.

To verify the particle model, a study by Meyerjürgens et al.[3] is used. In this study, floating surface drifters were developed and deployed in the German Bight, which registers its position every 10 minutes. 4 of the drifters were deployed in March of 2017, and another 3 in October of 2017. These drifters have a total depth of 506mm and a diameter ranging from 90 to 150mm. By design, the majority of the drifter resides under water.

As the drifters are relatively small and floating at the water surface, they can be interpreted as Lagrangian particles. There is an extensive dataset available of the trajectory of each drifter, and function as a tool to verify the particle model.

Ooms[4] used the drifters to verify if Lagrangian trajectories can be predicted using 2D water currents and Stokes drift. The model made poor predictions of the drifters positions, and the goal of this project is to verify whether the use of a 3D water current model improves the predictions.

3 Theory

3.1 Equations of motion

If the velocity of a Lagrangian particle is known, the equation of motion can be written as

$$dX_t = U dt \quad (1)$$

where X_t is the position of the particle at time t and U its velocity.

To solve for the particle velocity, Newton's second law is used[5]

$$M' \frac{dU}{dt} = F_a + F_w \quad (2)$$

where M' is the effective mass and F the acting forces on the particle. The subscripts a and w indicate the air and water force acting on the particle.

As a drifter buoy is floating with a small part above the water, both wind and water force affect the drifter. The part under water is affected by both general water motion, such as currents but also affects from the waves at sea. This effect is further explained in section 3.2.

Typically, for floating particles, the inertial term can be neglected[5], resulting in an equilibrium force equation for a particle,

$$\begin{aligned} 0 &= F_a + F_w \\ &= \frac{1}{2} C_{D_a} \rho_a A_a (u_a - u_p) |u_a - u_p| \\ &\quad + \frac{1}{2} C_{D_w} \rho_w A_w (u_w - u_p) |u_w - u_p|, \end{aligned} \quad (3)$$

where C_D is the drag coefficient, A the effective area and u the velocities. Here, u_p indicates the velocity of the particle.

Solving for the particle velocity[4], this results in

$$u_p = \frac{k_a u_a + k_w u_w}{k_a + k_w} \quad (4)$$

where $k_a = \sqrt{C_{D_a} \rho_a A_a}$ and $k_w = \sqrt{C_{D_w} \rho_w A_w}$.

3.2 Stokes drift

Many phenomena influence the velocity field of the water flow, such as tides, waves and estuaries. Ideally, all effects are included when calculating the velocity field. However, as this is infeasible due to computational limitations, estimation of these effects are made. Instead of calculating waves directly, a wave spectrum can be employed describing the statistical properties. By decoupling the waves from the calculation, there is no more interacting between the current and the waves. In reality, there is interaction and the aim is to model this by using Stokes drift.

Fluid particles on a wave do not travel in a closed orbit. In a closed orbit, the forwards and backwards velocity of a wave would cancel and after one period, the particle returns exactly to the same position. However, in propagating waves, there is a difference between the forwards and backwards velocity. This difference is called the Stokes drift, as it was first derived by G.G. Stokes. The net displacement of a particle by waves is on average as a result of this Stokes drift. This Stokes drift as a result of the waves is added to the velocity field to model the wave interaction. The particle velocity from eq. 4 then becomes

$$u_p = \frac{k_a u_a + k_w (u_c + u_s)}{k_a + k_w}, \quad (5)$$

where u_c is the current velocity and u_s the Stokes drift.

As mentioned before, instead of calculating the waves, a wave spectrum is can be to describe the statistical properties of the waves[6]. Using such a spectrum, waves can be described with minimal use of parameters. For an arbitrary spectral shape, the Stokes drift is dependent on the water depth and the vertical position in the water column. The equation for the Stokes drift is derived by Kenton[7] as

$$\mathbf{u}_s = g \iint_{-\infty}^{\infty} F(\mathbf{k}) \frac{\mathbf{k}}{\omega} \left[\frac{2k \cosh(2k(z+d))}{\sinh(2kd)} \right] d\mathbf{k} \quad (6)$$

where $F(\mathbf{K})$ is the wave spectral density, \mathbf{k} the wave number, z the z-coordinate and d the depth.

If the direction of the wave spectral density is separable, and the wave is unidirectional, equation 6 can be simplified, see appendix 6.1, resulting in the magnitude of the stokes drift in the wave direction as

$$u_s = \frac{16\pi^3}{g} \int_0^\infty f^3 F_f(f) e^{\frac{8\pi^2 f^2 z}{g}} df \quad (7)$$

where f is the frequency. As the drifters are floating objects, $z \rightarrow 0$ and as a result, the integral in eq. 7 becomes the third moment of a given wave spectral density[8], resulting in

$$u_s = \frac{16\pi^3}{g} \int_0^\infty f^3 F_f(f) df = \frac{\pi^3 H_{m0}^2}{g T_3^3} \quad (8)$$

where H_{m0} and T_3 represent the significant wave height and the third period respectively.

3.3 JONSWAP

The wave spectrum used to solve the Stokes drift in this project is the one found by the Joint North Sea Wave Project (JONSWAP)[9]. During this project, the North sea was observed for several weeks, and empirically found a wave spectral density depending only on the peak frequency.

The JONSWAP spectrum also gives more insight other statistical properties, such as periods. As the third period T_3 in eq. 8 is not measured often, the JONSWAP spectrum can be utilized in order to estimate the Stokes drift using the peak frequency[8]:

$$T_3 \approx 0.680 \frac{1}{f_p} = 0.680 T_p \quad (9)$$

resulting in

$$u_s = 3.18 \frac{\pi^3 H_{m0}^2}{g T_p^3}. \quad (10)$$

Since the drifters do not necessarily reside in deep waters, but in waters ranging from 10-30m most of the time, the validity has to be checked for these depths, see appendix 3.2. As the comparison between the arbitrary depth and the deep water in fig. 1 shows, the validity of the approximation is dependent on the peak period.

Note that in practice, the Stokes drift rarely increases in such a rate as in figure 1, as this is an approximation using an unidirectional wave field. In many cases, loss off Stokes drift is a result off energy loss in directions then the dominant Stokes direction. Furthermore, coastal effects such as undertow and shoaling influence the Stokes drift. However, as the studied area of the drifters mainly has a depth of more than 10m, the deep water approximation is valid.

The equation 10 is an approximation of the Stokes drift at $z = 0$. However, the exponent in eq. 7 suggest a decrease in the magnitude as z decreases and is dependent of the peak frequency. To check the rate of this, z is chosen at the center of the drifter, thus $z = -0.25m$. The resulting reduction factor is displayed in figure 2.

3.4 Diffusivity

Theoretically, the exact velocity and therefore the trajectory of a particle can be calculated. However, due to unresolved physics, this is not the case. Therefore, stochastic noise is added to the motion, such that eq. 1 will become a stochastic differential equation (SDE). [10]

For a general trajectory $\mathbf{X}(t)$, the SDE is given by

$$dX_i(t) = a_i(t, \mathbf{X}_t) dt + \sigma_{ik}(t, \mathbf{X}_t) dW_k(t) \quad (11)$$

where a_i is the drift and σ_{ik} the diffusivity coefficient tensor. $W_k(t)$ is a Wiener process. The increment $dW_k(t) = W(t+dt) - W(t)$ is Gaussian distributed, with a mean zero and variance dt . However, this is not exactly the equation used in this project.

As we are interested in where particles might end up, the probability density function (PDF) for the particles is required and how it evolves over time. As we describe X_t as an Itô process, a particle ensemble

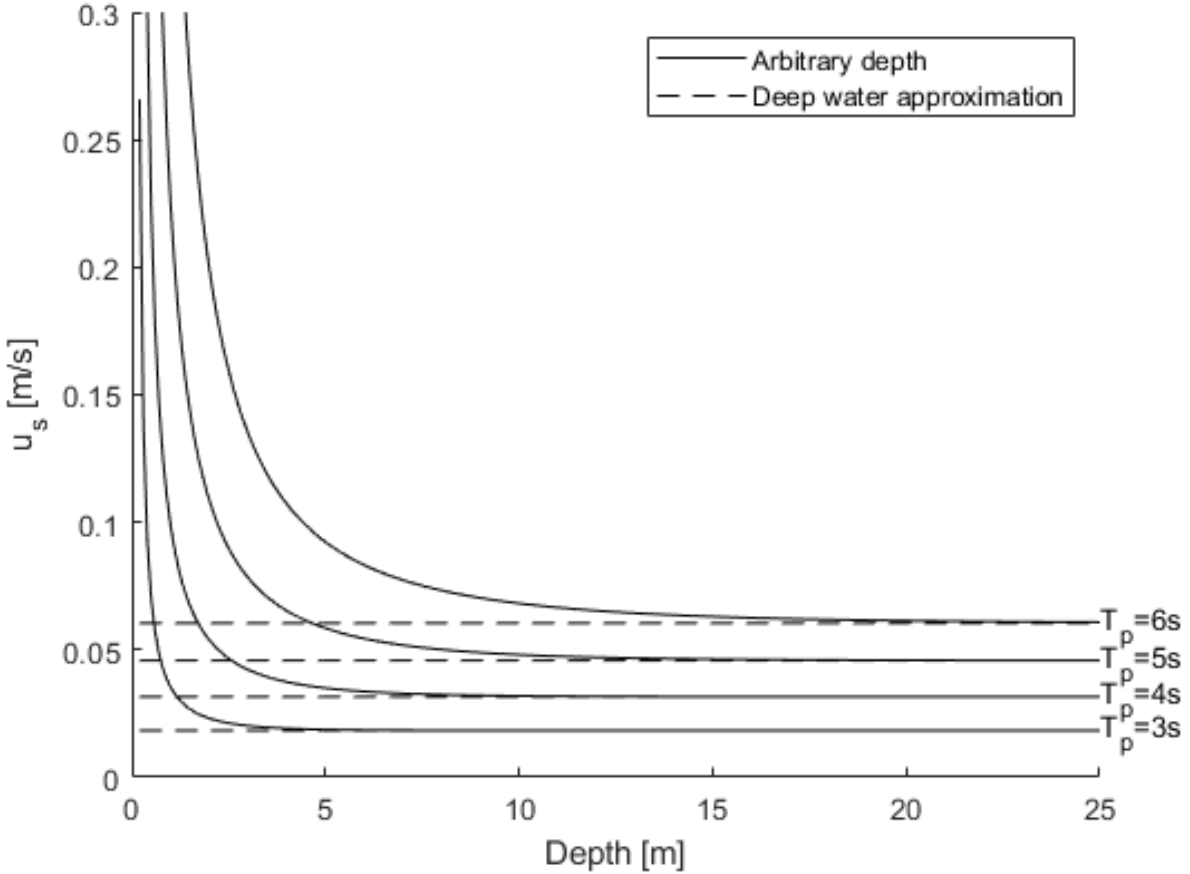


Figure 1: Numerical solution for the Stokes drift for various peak periods T_p , typical for the German Bight, where $T_p = \frac{1}{f_p}$ using the unidirectional form of eq.6 (see eq. 36) for arbitrary depth and eq.7 for the deep water approximation using $z = 0.25m$.

of this process will describe this PDF. The Itô form of the Fokker-Planck equation describes the evolution of the PDF;

$$\frac{\partial P}{\partial t} = \partial_i(a_i P) + \partial_{ij}(K P) \quad (12)$$

and the corresponding SDE for the trajectory is given by[10]

$$dX_i(t) = (U_i + \partial_j K)dt + \sqrt{2K}dW_i(t), \quad (13)$$

where i indicates the component in the i direction, K is a diffusion coefficient and U the particle velocity as described by eq. 5

To give an estimation of the probability density function from a particle ensemble at a given time, a bivariate kernel density estimation is used. At a given time t , the position of particle k is denoted by $\mathbf{X}_k(t)$, and the kernel density estimation is then calculated as

$$\hat{f}(\mathbf{x}, t) = \frac{1}{n} \sum_{k=1}^n f(\mathbf{x} - \mathbf{X}_k(t)) \quad (14)$$

where f is a bivariate probability density function and n the number of particles. In this case, a bivariate normal density function is used, with $\sigma^2 = 50m$. In other words, this kernel density estimation is a summation of normal pdf's, where $\mu = \mathbf{X}_i(t)$ and $\sigma^2 = 50m$.

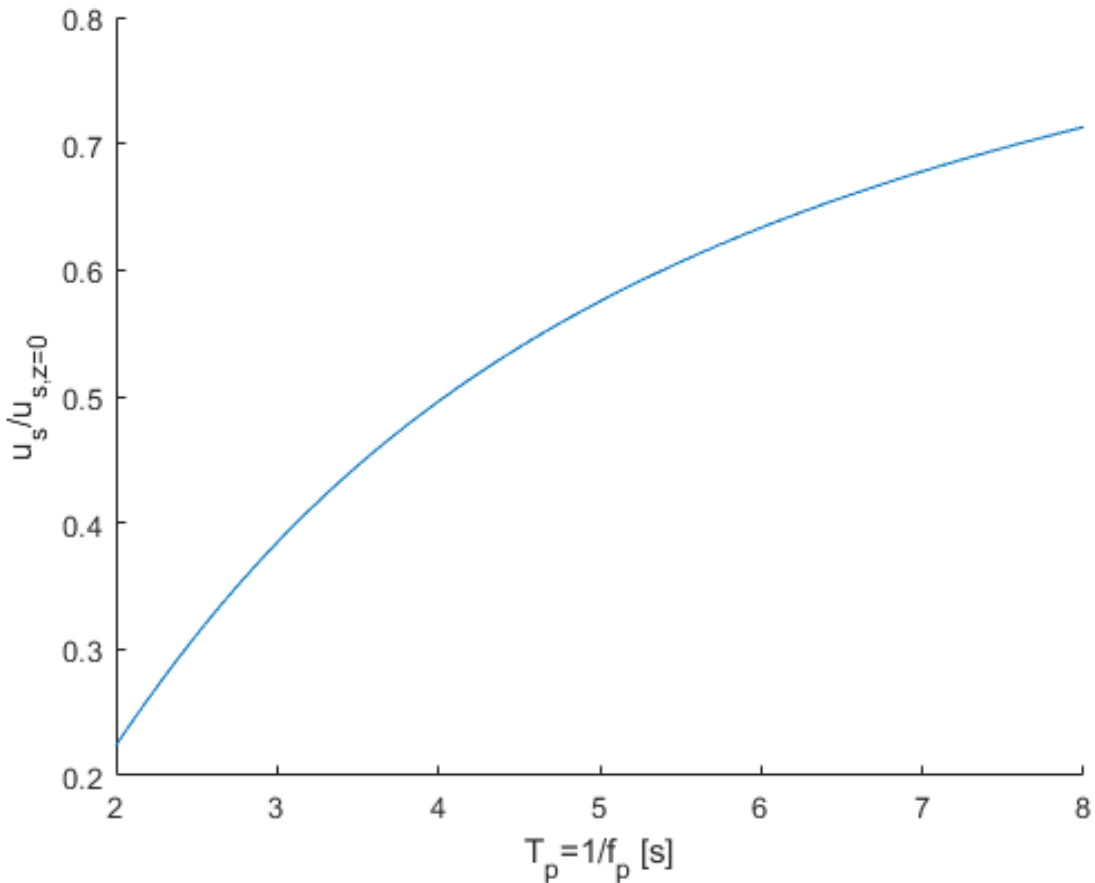


Figure 2: Numerical solution of eq. 7. The normalized reduction factor of the Stokes drift for various peak periods T_p , where $T_p = \frac{1}{f_p}$ where $z = -0.25m$.

3.5 Eddy viscosity

The diffusion above is not molecular diffusion, but diffusion as a result of turbulence. If every pocket of fluid would flow in the same direction with the same velocity, there would be no turbulence. However, in a turbulent flow, this is not the case. Due to the variations in direction and velocities, swirls emerge, called eddies. In the ocean, these eddies exists in wide variety of sizes, both in the horizontal and vertical direction. Horizontally, the larger ones exists of hundreds kilometers and are limited by the size of the ocean. The smaller ones can be centimeters and are limited by the Kolmogorov microscales, the smallest possible turbulent scales. In time, these turbulent scales can range from minutes up to decades and even longer[11].

Therefore, it is practically impossible too numerically solve this on all scales. However, since turbulence is chaotic, it can be simulation using noise, as described in the previous section. The noise depends on the amount of turbulence, represented by the Eddy diffusion coefficient.

In this particular case, not the eddy diffusion but the eddy viscosity coefficient is used. The ratio between these two coefficient is represented by the turbulent Prandtl number. A common estimation for this number is $Pr_b = 1$ [12], which means the Eddy viscosity and diffusion have the same value.

The horizontal eddy viscosity coefficient is a characteristic of the flow field, and can be estimated by this flow. Many models are available and here the Smagorinsky model is used. In this model, the Eddy viscosity is given by[13]

$$\nu_T = (C_s \Delta)^2 |\bar{S}| \quad (15)$$

where $|\bar{S}| = \sqrt{2\bar{S}_{ij}\bar{S}_{ij}}$ is the magnitude of the strain-rate tensor, C_s the Smagorinsky model and Δ the filter width. An additional background viscosity ν_b is added, and the strain-rate tensor is calculated from the flow, resulting in

$$\nu_T = \nu_b + (C_s \sqrt{\Delta x \Delta y})^2 \sqrt{2 \frac{\partial u}{\partial x}^2 + \left(\frac{\partial u}{\partial y} + \frac{\partial v}{\partial x} \right)^2 + 2 \frac{\partial v}{\partial y}^2} \quad (16)$$

where (u, v) is the flow. In this particular case, $\nu_b = 0.1 m^2/s$ and $C_s = 0.1$ are chosen.

3.6 Finite time Lyapunov exponent

A good understanding in the behavior of the water in the German Bight, in particular the period when the drifters were in the water, is necessary to correctly predict particle trajectories in this area. In mathematics, one characteristic for a dynamic system, is the Lyapunov exponent. It gives insight in the sensitivity of the initial condition.

Take two trajectories, initially infinitesimally close together. We denote \mathbf{X}_0 and $\mathbf{X}_0 + \delta\mathbf{X}_0$ as the initial positions of these two trajectories. As the trajectories evolve over time, they might diverge from one another. Within the linear approximation, the distance between the trajectories can be expressed using the initial distance

$$|\delta\mathbf{X}(t)| \approx e^{\lambda t} |\delta\mathbf{X}_0|. \quad (17)$$

The new parameter λ describes the rate off this change in distance between the trajectories. If $\lambda > 0$, the distances increases and the trajectories diverge. This characteristic parameter λ is called the Lyapunov exponent. Note that generally, λ can vary depending on the orientation of $\delta\mathbf{X}_0$, and the maximum λ is referred to as the Lyapunov exponent.

The Lyapunov exponent is therefore defined as

$$\lambda = \lim_{t \rightarrow \infty} \lim_{|\delta\mathbf{X}_0| \rightarrow 0} \frac{1}{t} \ln \frac{|\delta\mathbf{X}(t)|}{|\delta\mathbf{X}_0|}. \quad (18)$$

In order to get a better insight in the behavior of the water in the German Bight, we will calculate the Lyapunov exponent. In practice however, the above expression, eq.18 is not possible as we have a finite time interval and a discrete velocity of finite resolution. Therefore, slightly different variant is explored, the finite time Lyapunov exponent[14].

For a two-dimensional divergence-free flow, which is the case in an incompressible flow, the separation $\delta\mathbf{X}(t)$ evolves in time as

$$\dot{\delta\mathbf{X}}(t) = S(t)\delta\mathbf{X}(t) \quad (19)$$

where S is the Jacobian of the flow

$$S(t) = \begin{pmatrix} \partial_x u & \partial_y u \\ \partial_x v & \partial_y v \end{pmatrix} \quad (20)$$

which is evaluated along the trajectory $\mathbf{X}(t)$.

To estimate the finite time Lyapunov exponent, take an infinitesimal circle which will deform along the trajectory $\mathbf{X}(t)$. The deformation $M(t)$ evolves as

$$\dot{M} = SM \quad (21)$$

where M is initially the identity matrix. As the matrix M can be calculated over time, the maximum eigenvalue m of the matrix $M^T M$ can also be calculated. Using this eigenvalue m , the finite time Lyapunov exponent is expressed as

$$\lambda(\mathbf{X}(t), t) = \frac{1}{2t} \ln(m) \quad (22)$$

where the long time standard deviation decreases[15] over time as

$$\sigma \sim t^{-\frac{1}{2}}. \quad (23)$$

Table 1: Initial position of the measured drifters from the study by Meyerjürgens et al.[3].

	Initial time	Latitude	Longitude
Drifter 1[16]	2017-03-13T21:25	53.78377	6.34169
Drifter 2[17]	2017-03-13T21:24	53.78372	6.34109
Drifter 3[18]	2017-03-14T13:17	53.75972	7.65082
Drifter 4[19]	2017-03-14T13:18	53.76004	7.65037
Drifter 5[20]	2017-10-10T19:01	54.05001	7.95421
Drifter 6[21]	2017-10-10T18:56	54.04210	7.95985
Drifter 7[22]	2017-10-13T05:46	53.81080	7.68867

4 Results

4.1 Velocity datasets

Modeling the particles as described, wind and water velocities are required. To obtain this data, the DCSM-FM 3D model is used from the software package Delft3D-FM. This model uses a fixed grid, and the water and wind velocity is calculated on each cell, where $\Delta t = 1\text{hour}$. At a given time, the position of the particle determines in what cell it resides. Determining the water and wind velocities for that particle, the cell values are used. In time, a linear interpolation method is used, and in space no interpolation is used.

A representation of the surface water direction, calculated using the 3D velocity field is displayed in figure 3. Since the directions are highly dependent on the tide, two figures are shown six hours apart.

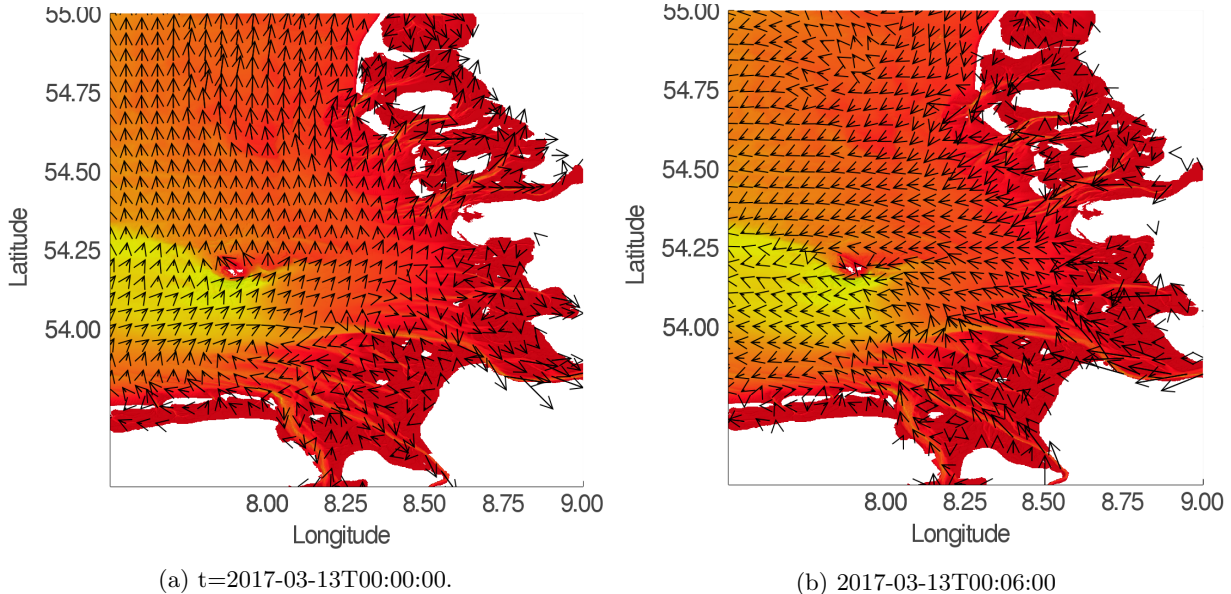


Figure 3: Surface water velocity in the German Bight at times 6 hours apart, from the 3D water velocity model.

To calculate the Stokes drift, the significant wave height H_s and the mean period T_m were retrieved from a SWAN DCSM model.

4.2 Drifter datasets

During this project, the measurements of the drifter trajectories come from the study by Meyerjürgens et al.[3]. In this study, 7 drifters were tracked in the German Bight in 2017, denoted by the number 1-7. The initial positions of the drifters are displayed in table 1.

4.3 Simulations

Using the stochastic differential equation 13 and the eddy viscosity equation 16, the water velocity can be estimated. Combined with the wind velocity and the Stokes drift, the particle trajectories can be calculated. For each drifter, $n = 300$ particles are used with an initial position equal to that of the drifter, see table 1. As drifter 1 and 2 are initially close to each other, the results of the simulations are displayed in the same figure. The same holds for drifter 3 and 4, and drifter 5 and 6.

In the following sections, results are displayed of simulations using 3 different settings. At first, simulations are performed excluding the Stokes drift, thus $u_s = 0$.

Secondly, the Stokes drift is included. Tang et al.[15] found that the mean Stokes drift can be estimated using a wind velocity percentage, ranging from 0.5% for low velocities and 2.1% for high velocities. Ooms[4] found that for this particular case, 1.6% is a good estimation. To compare the performance for the simulations including Stokes drift, both estimations are compared. As the Stokes drift is dependent of depth and peak frequency, the reduction factor displayed in figure 2 is used.

At last, the calculations are performed backwards in time. In many cases, one is interested in the origin of a particle given its destination. Given the destination of the drifters, an estimation of the origin is calculated and compared to the actual origins.

In each figure, a bathymetry is displayed of the German Bight. This gives a representation of the Bathymetry, but is not necessarily a representation of the bathymetry used in the flow calculations, as this is an external resource[23]. In these figures, a trajectory of a particle is indicated in green. This is not a random trajectory of a particle, but the trajectory with the smallest Euclidean distance to the drifter trajectory (indicated in black). A discrete constant timestep $\Delta t = 100s$ is used, and \mathbf{X}_i is known at discrete times $t_0, t_0 + \Delta t, \dots, t_{end}$. The trajectory \mathbf{X}_i for which

$$d(\mathbf{X}_i, \mathbf{X}_{drifter}) = \min_i \sum_{t=t_0}^{t_{end}} \|\mathbf{X}_i(t) - \mathbf{X}_{drifter}(t)\|_2 \quad (24)$$

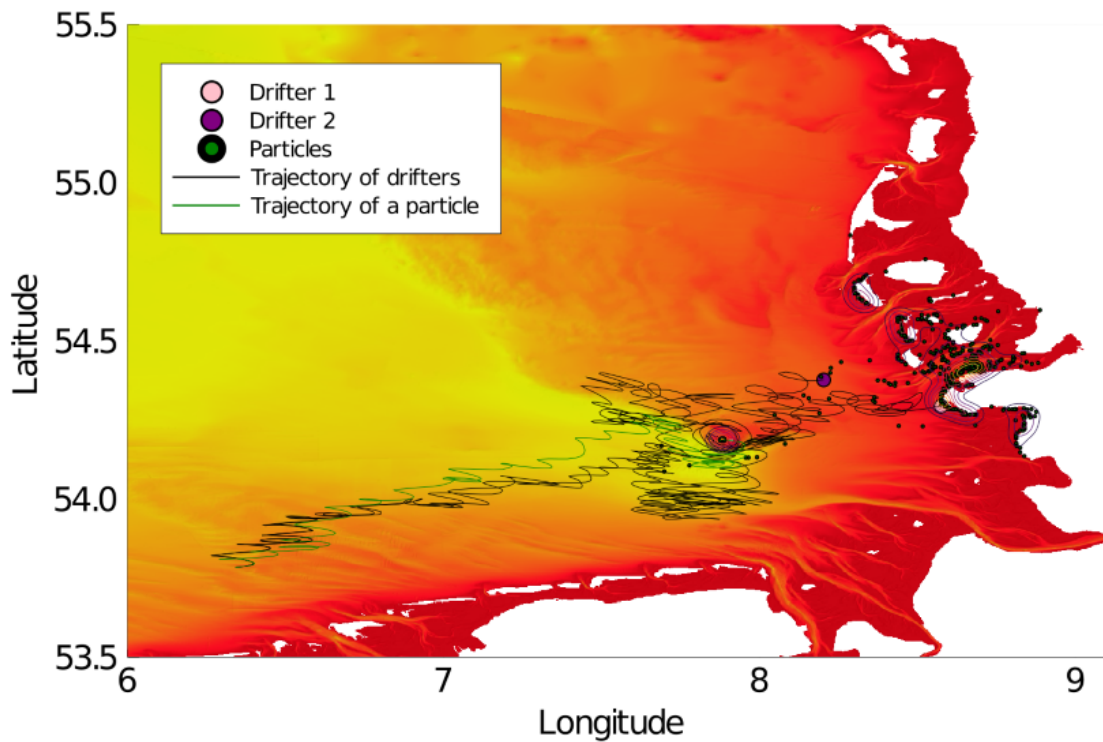
is selected and displayed as the green line in each figure.

4.3.1 Simulation without Stokes drift

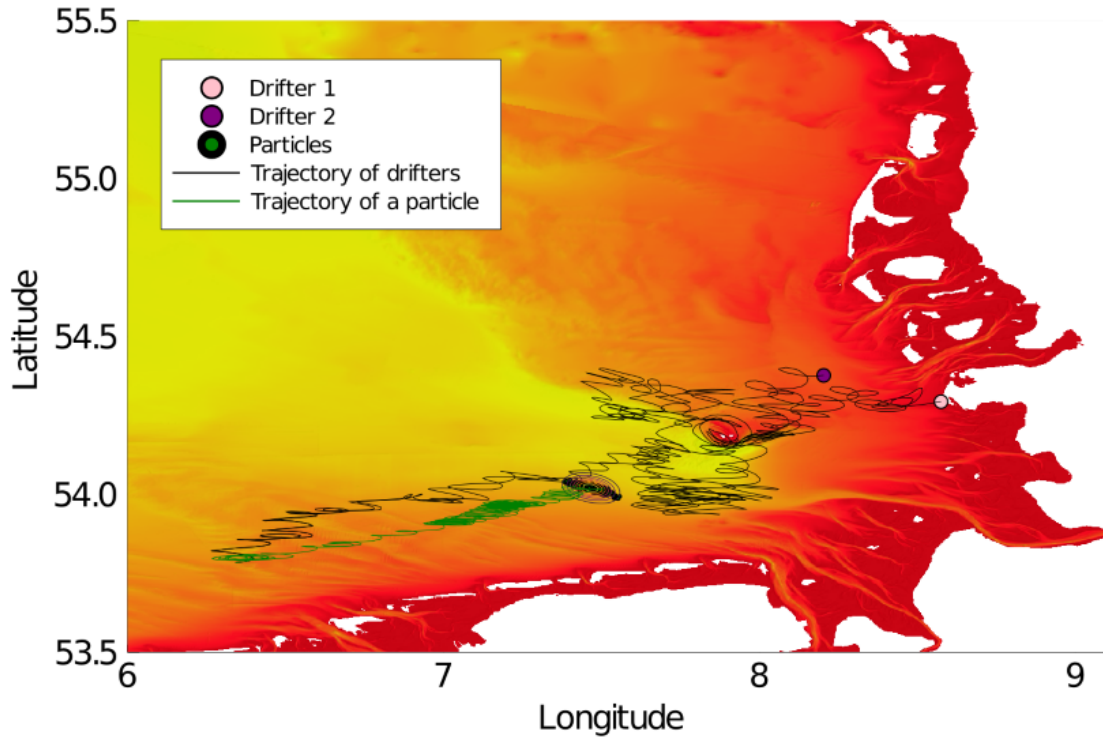
At first, simulations without additional Stokes drift were executed, thus using $u_s = 0$. The results of the simulations using the 3D and 2D velocity field are displayed in (a) and (b) of figure 4-7 respectively. From this result, it can be observed that the use of a 3D velocity field improves the results in comparison to the 2D velocity field. There is still a wide spread between the particles which can be the result of a high diffusion coefficient K . However, as is also displayed in the first 3 figures, two drifters initially close together, have a similar large distance between them.

Overall, the calculations using the 3D velocity field are accurate in estimating the positions of the drifters. However, as can be observed in figure 4a, the trajectory of the particle near the island Helgoland have a different trajectory as the observed drifter. This indicates an inaccuracy in the water flow near the island. As the model predicts the drifters away from the island accurately, improving and updating the water velocities in this area might improve the predicted trajectories.

Since the fraction in eq. 5 is mainly water ($\frac{k_w}{k_w+k_a} \approx 0.998$), it is expected that the results from 4-7 are a representation of the Lagrangian properties in this area. To verify this claim, the simulation without wind are performed $u_p = u_w$, resulting in similar results. For more detail, see appendix 6.3.

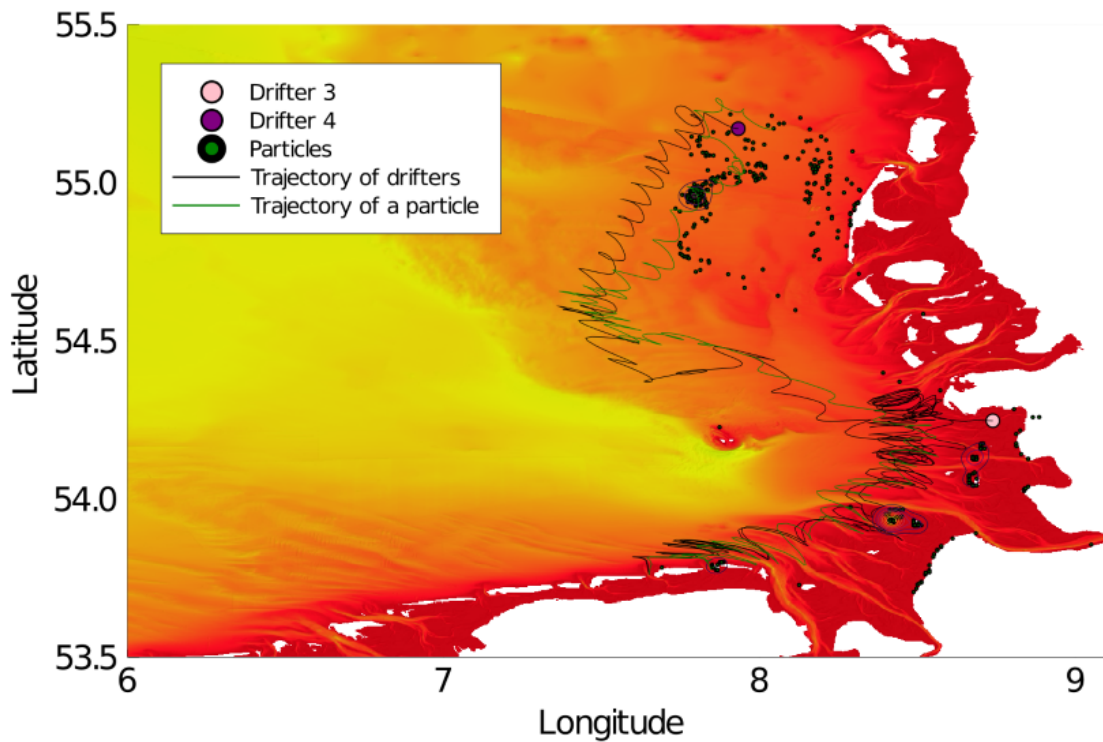


(a) Using the 3D velocity field.

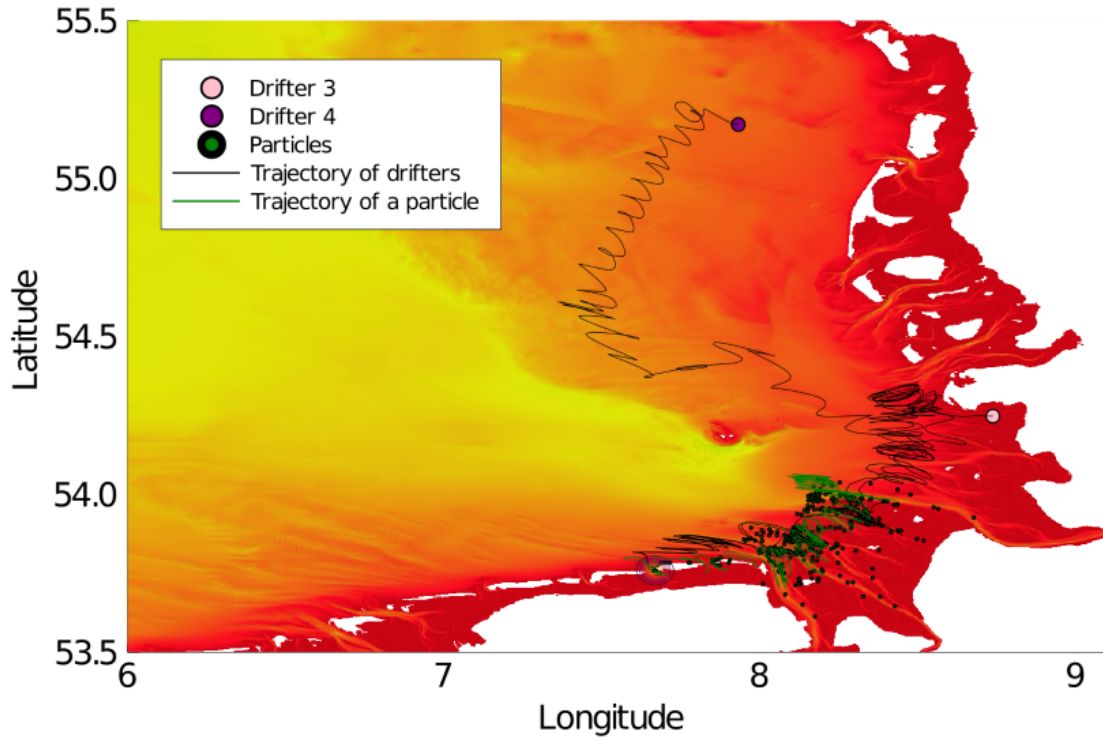


(b) Using the 2D velocity field.

Figure 4: Simulations of particles at time 2017-04-15T15:10, 300 particles initially at position of drifter 1, and 300 at the position of drifter 2. For the particle velocity, eq. 5 is used where $u_s = 0$ (no Stokes drift).

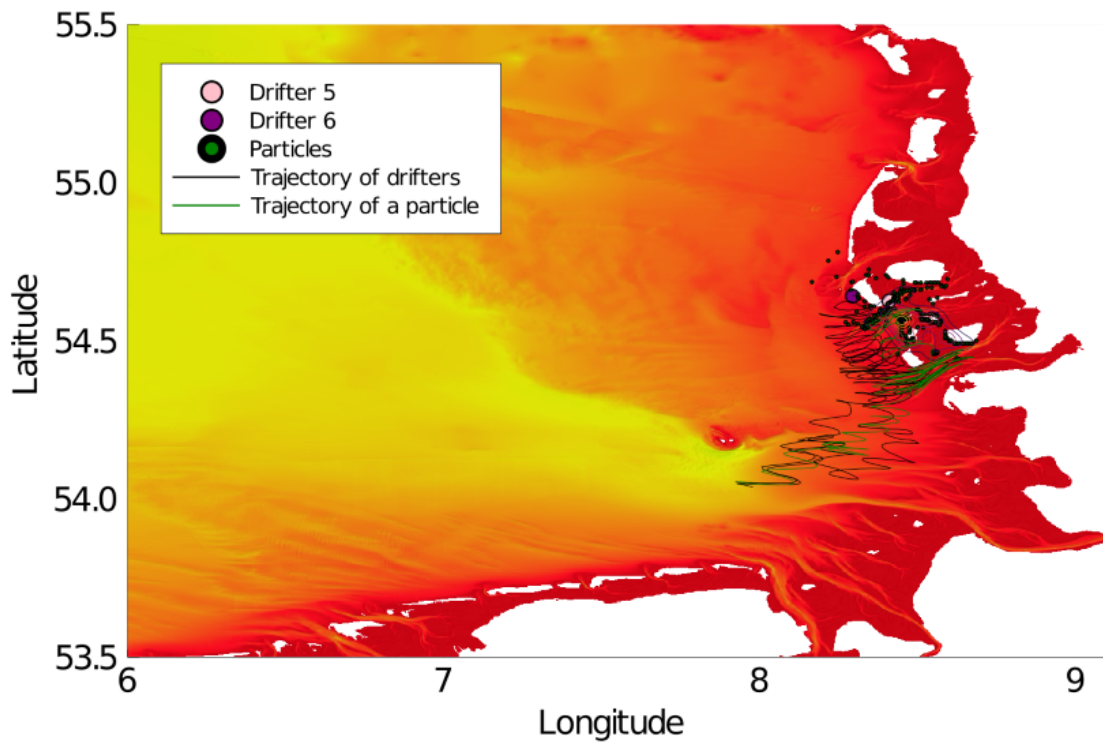


(a) Using the 3D velocity field.

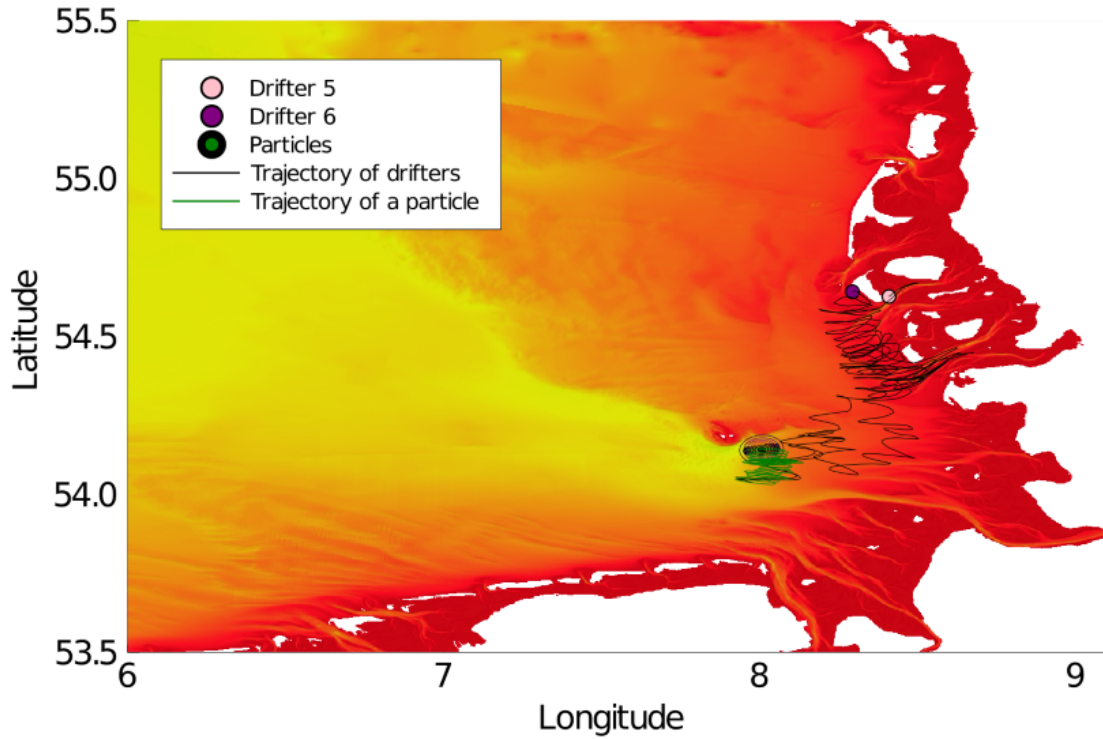


(b) Using the 2D velocity field.

Figure 5: Simulations of particles at time 2017-04-05T20:57, 300 particles initially at position of drifter 3, and 300 at the position of drifter 4. For the particle velocity, eq. 5 is used where $u_s = 0$ (no Stokes drift).

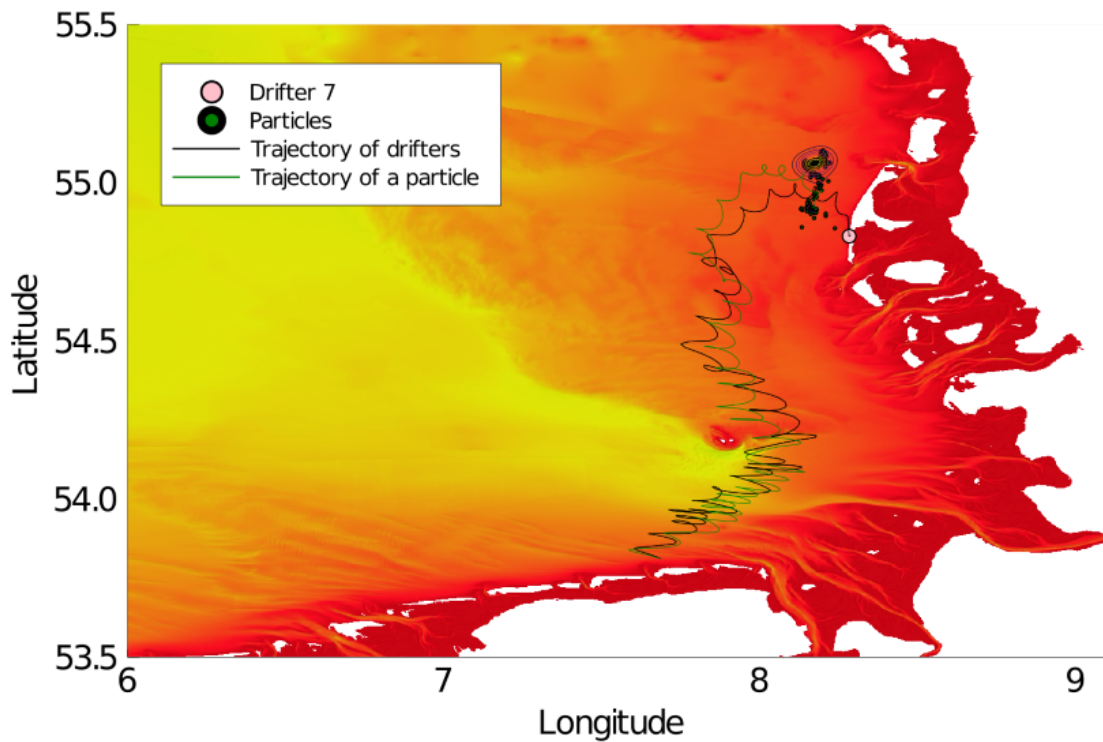


(a) Using the 3D velocity field.

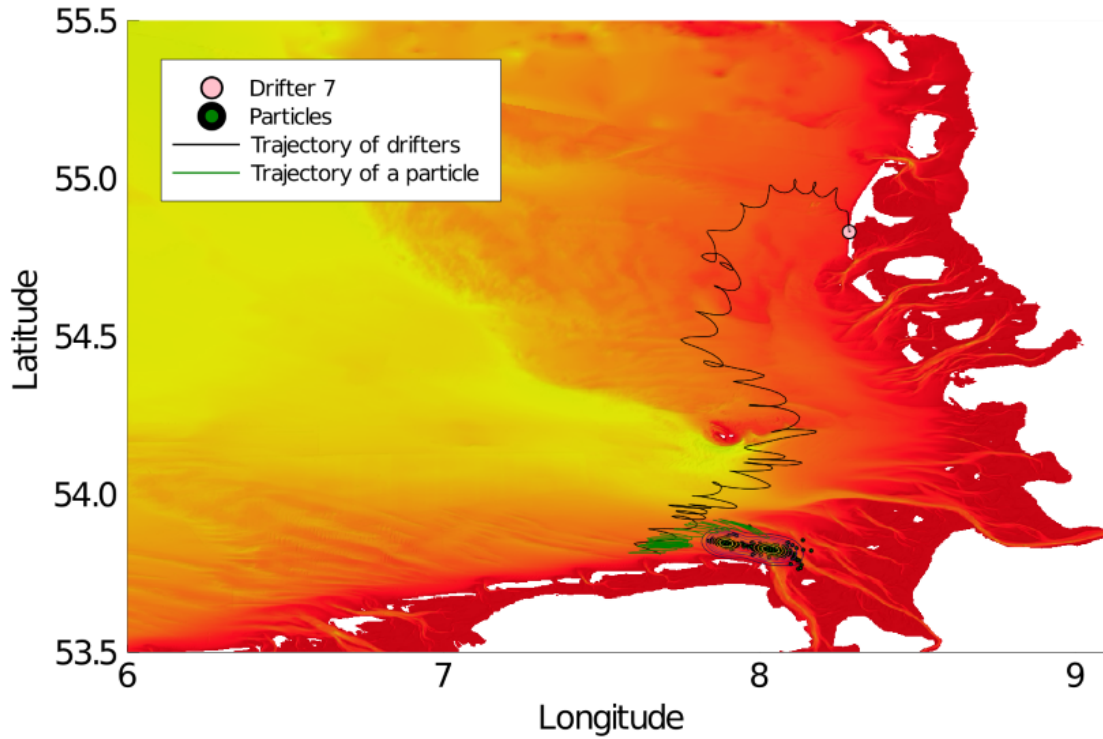


(b) Using the 2D velocity field.

Figure 6: Simulations of particles at time 2017-10-23T07:53, 300 particles initially at position of drifter 5, and 300 at the position of drifter 6. For the particle velocity, eq. 5 is used where $u_s = 0$ (no Stokes drift).



(a) Using the 3D velocity field.



(b) Using the 2D velocity field.

Figure 7: Simulations of particles at time 2017-10-27T12:58, 300 particles initially at position of drifter 7. For the particle velocity, eq. 5 is used where $u_s = 0$ (no Stokes drift).

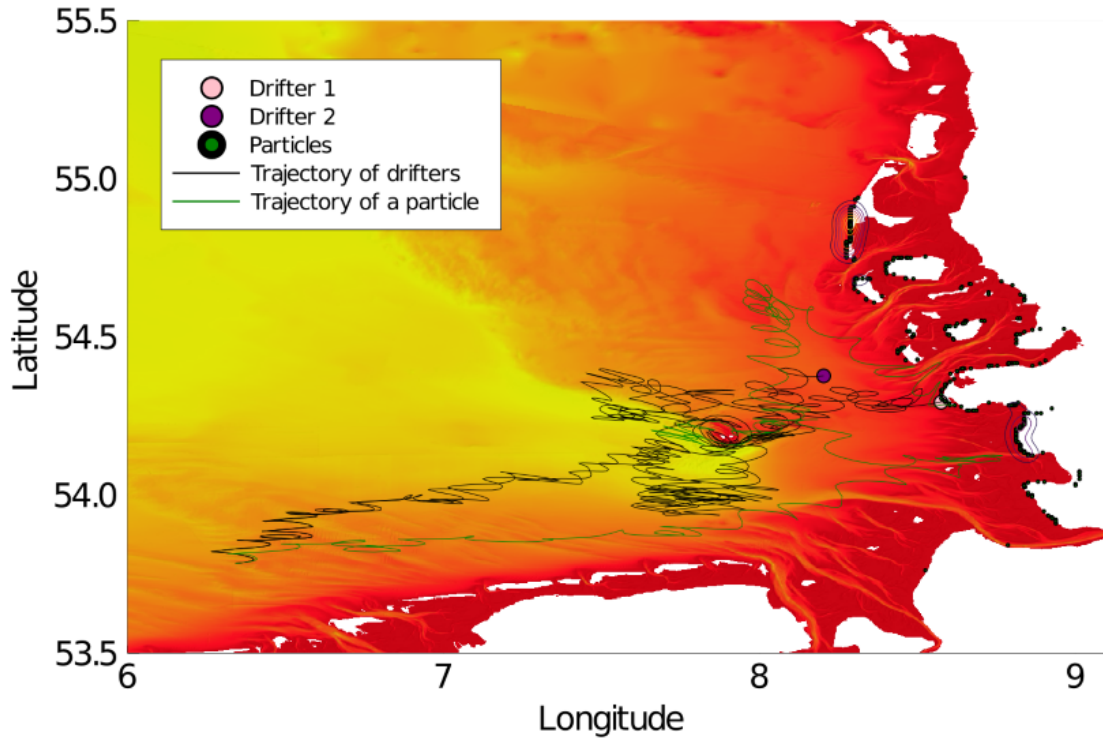
4.3.2 Simulations including Stokes drift

Next, the simulations are performed including the Stokes drift. Therefore, eq. 5 is used where u_s is the Stokes drift. In figures 8-15, the results are displayed for both the Stokes drift estimated with the JONSWAP spectrum and the 1.6% wind.

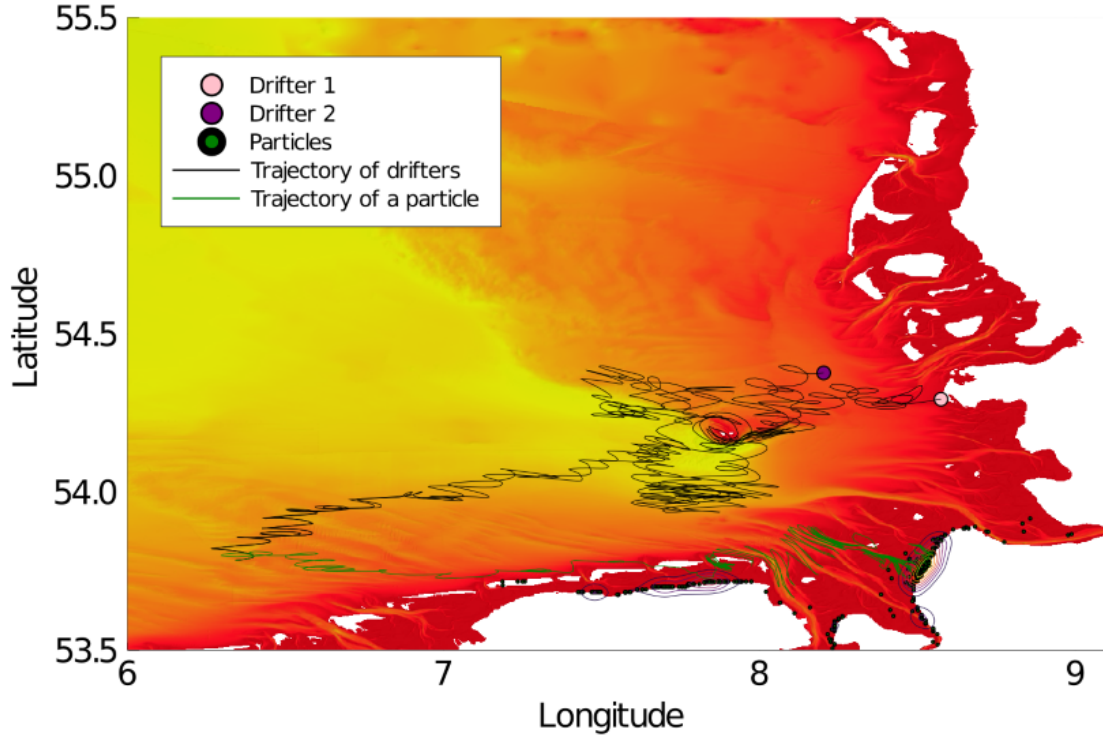
It can be observed, that for the 2D velocity field, the additional velocity as a result from the Stokes drift give the trajectories more similarity to the measured drifters. However, as these modeled particles have velocities higher than the drifter, the particles reach the shore long before the drifter. The Stokes drift is therefore not a improvement from the previous section.

For the 3D velocity field, the additional Stokes drift gave poor results. There are still particles with an trajectory close to the drifter, but the majority of the particles already stranded before the drifters reach the shore. Again, this suggest that magnitude of the Stokes drift was too big.

In its current form, the Stokes drift does not improve the results. However, excluding the Stokes drift entirely can not be concluded from this, as many more assumptions and approximations are made during this report. For the derivation of the Stokes drift, the assumption of a unidirectional wave was used. This might be accurate for ocean waves, but in and near a coastal area, this might not be the case, resulting in a loss of Stokes drift[8]. This suggest that nonlinear effects have a bigger impact on the Stokes drift than assumed. This is also observed by Clifford[24].

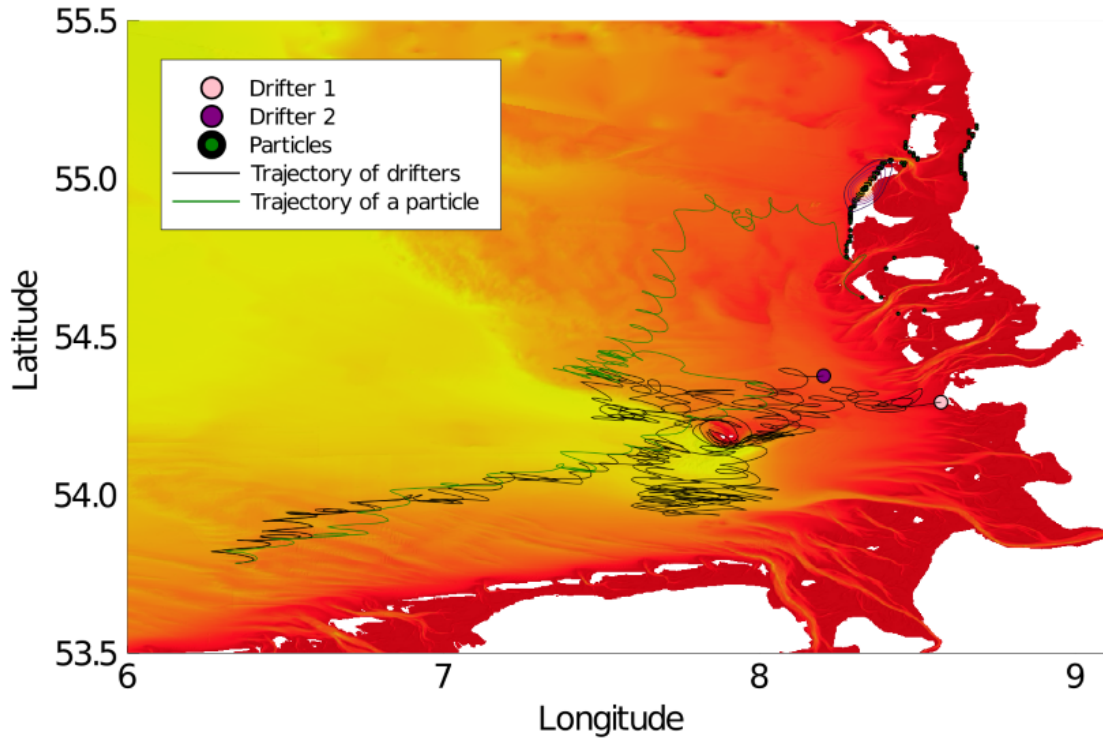


(a) Using the 3D velocity field.

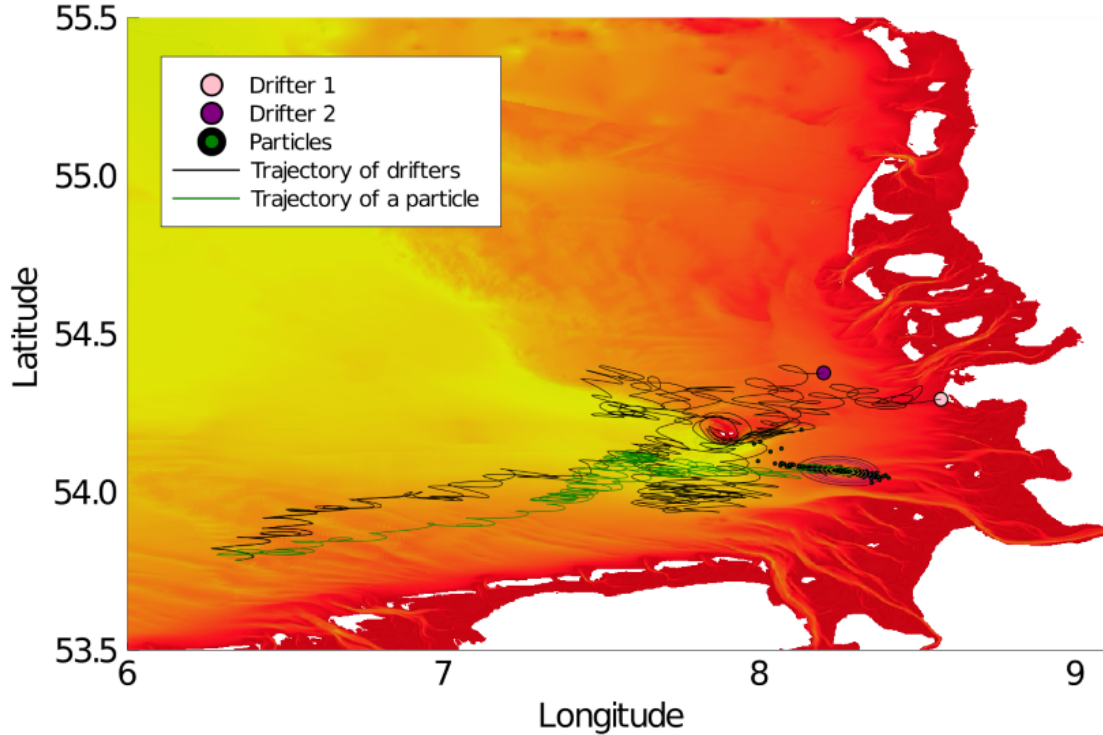


(b) Using the 2D velocity field.

Figure 8: Simulations of particles at time 2017-04-15T15:10, 300 particles initially at position of drifter 1, and 300 at the position of drifter 2. For the particle velocity, eq. 5 is used where $u_s = u_{s,jonswap}$, the Stokes drift estimated using the JONSWAP spectrum, eq 8.

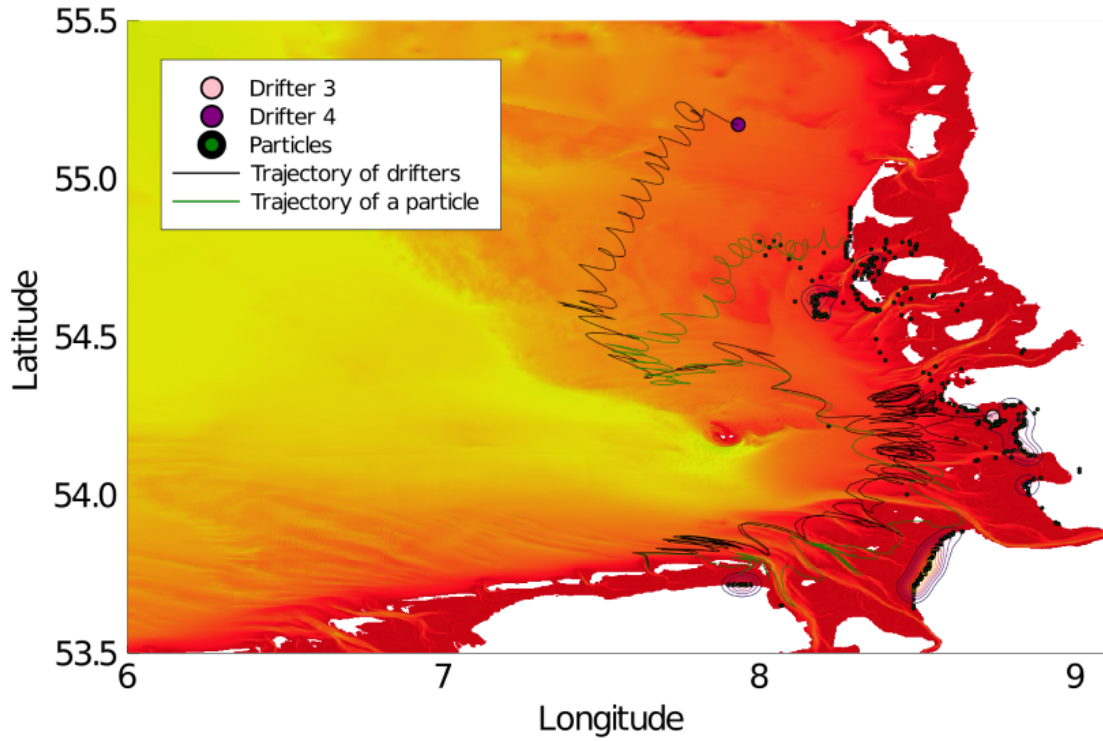


(a) Using the 3D velocity field.

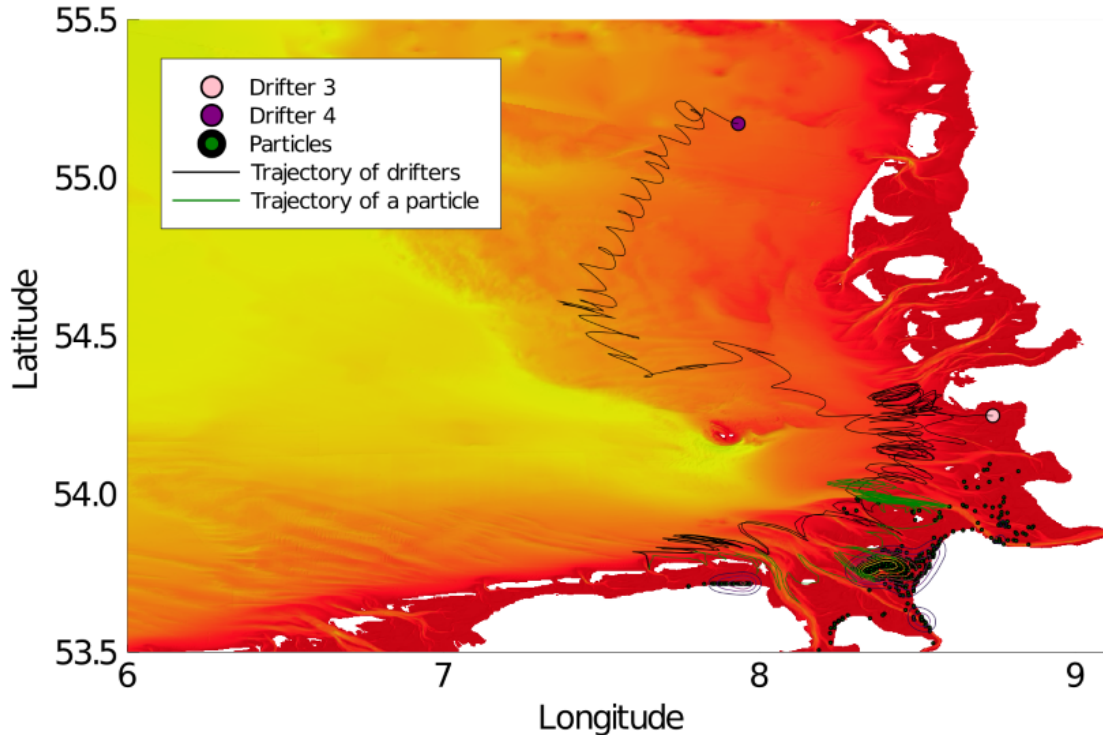


(b) Using the 2D velocity field.

Figure 9: Simulations of particles at time 2017-04-15T15:10, 300 particles initially at position of drifter 1, and 300 at the position of drifter 2. For the particle velocity, eq. 5 is used where $u_s = 1.6\%u_a$, the Stokes drift estimated using the 1.6% wind estimation.

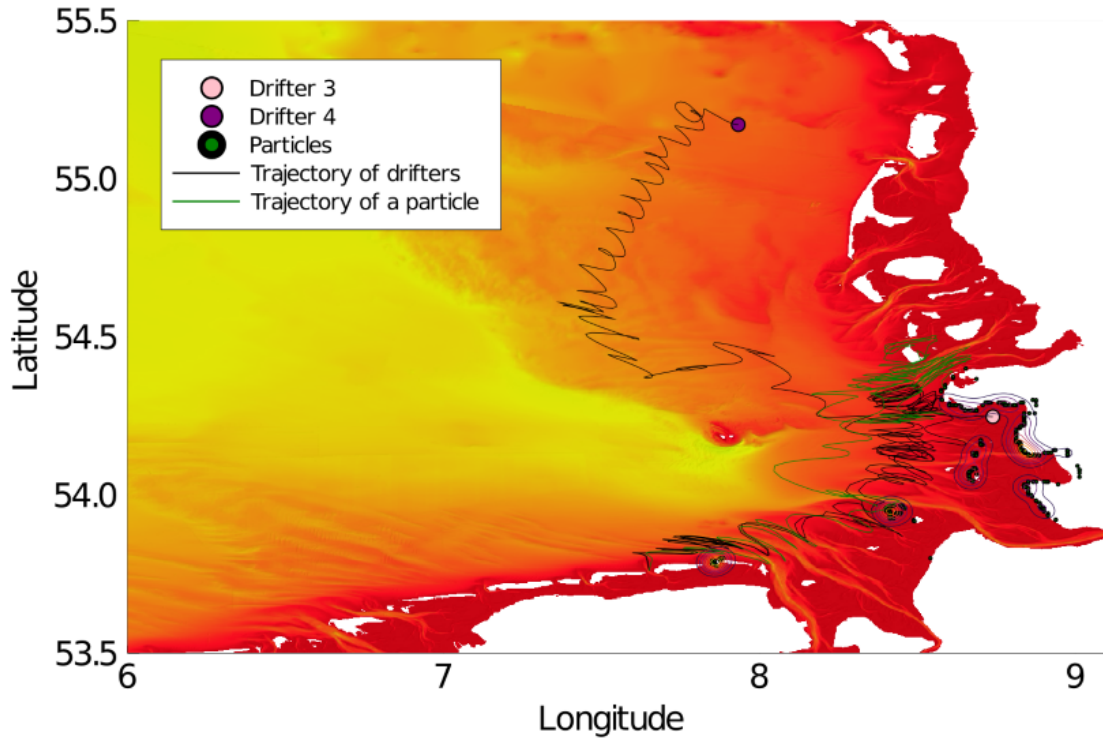


(a) Using the 3D velocity field.

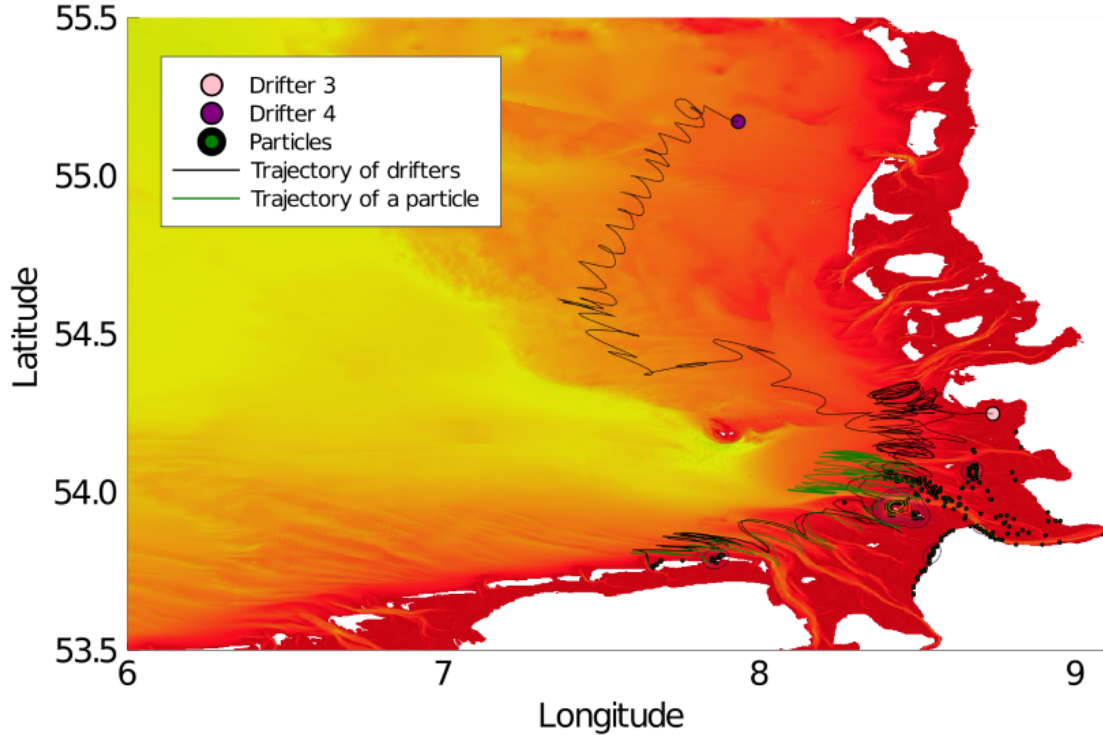


(b) Using the 2D velocity field.

Figure 10: Simulations of particles at time 2017-04-15T15:10, 300 particles initially at position of drifter 3, and 300 at the position of drifter 4. For the particle velocity, eq. 5 is used where $u_s = u_{s,jonswap}$, the Stokes drift estimated using the JONSWAP spectrum, eq 8.

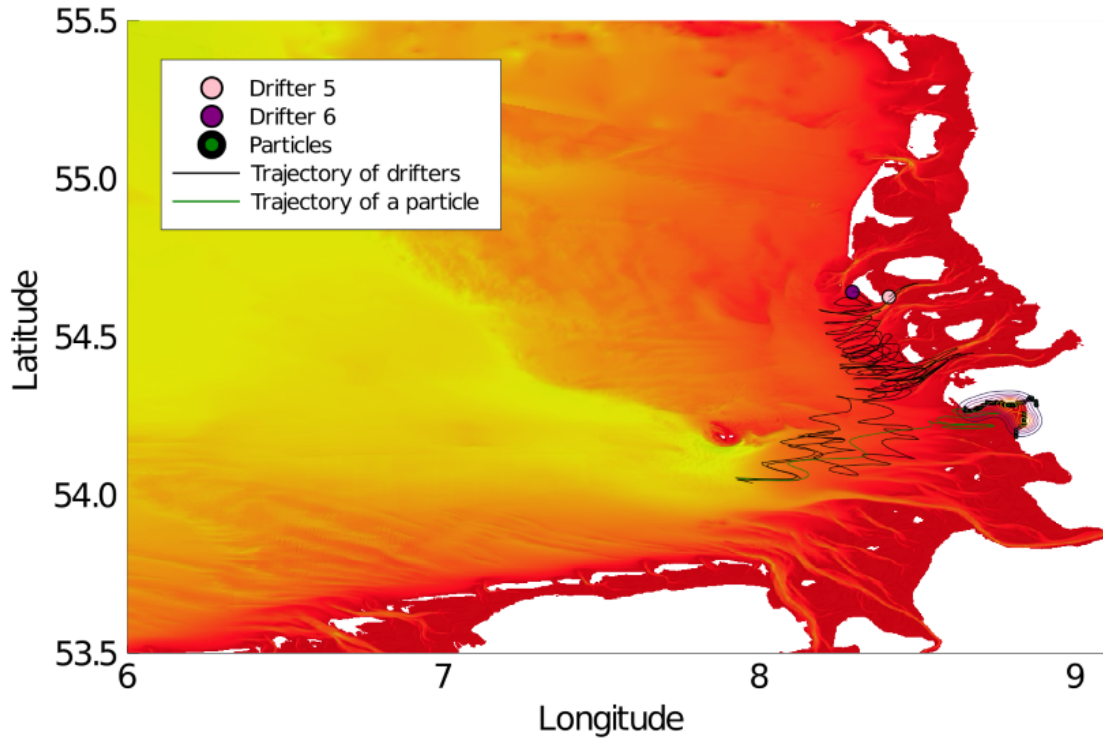


(a) Using the 3D velocity field.

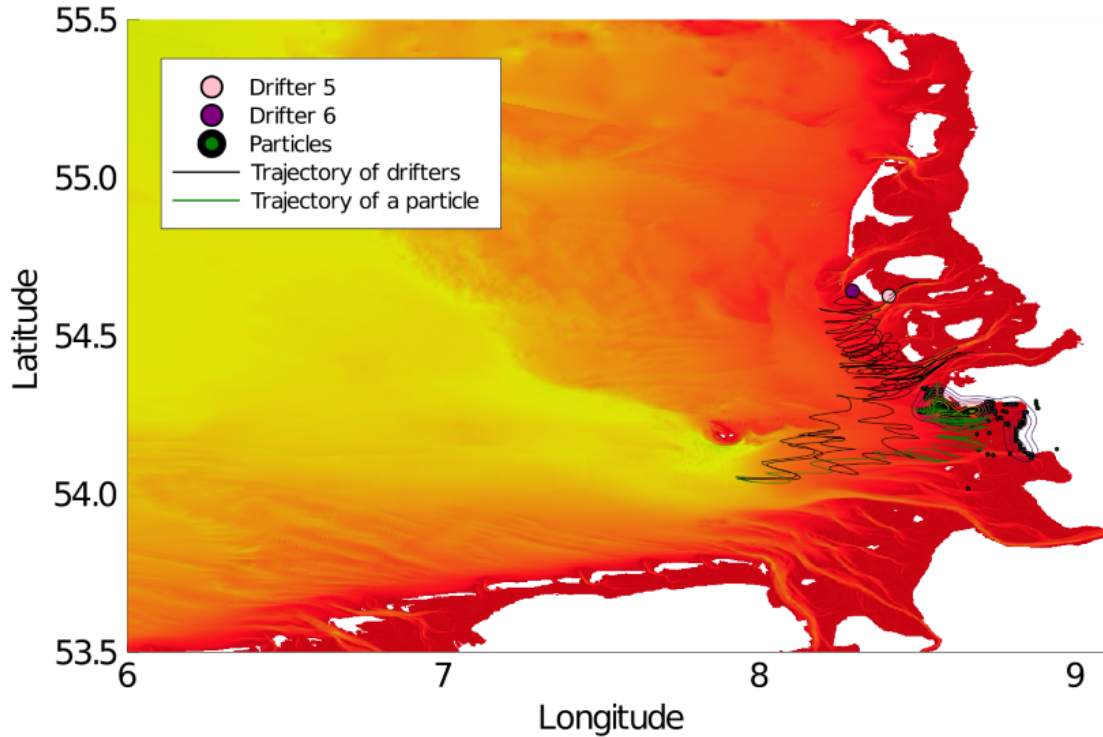


(b) Using the 2D velocity field.

Figure 11: Simulations of particles at time 2017-04-05T20:57, 300 particles initially at position of drifter 3, and 300 at the position of drifter 4. For the particle velocity, eq. 5 is used where $u_s = 1.6\%u_a$, the Stokes drift estimated using the 1.6% wind estimation.

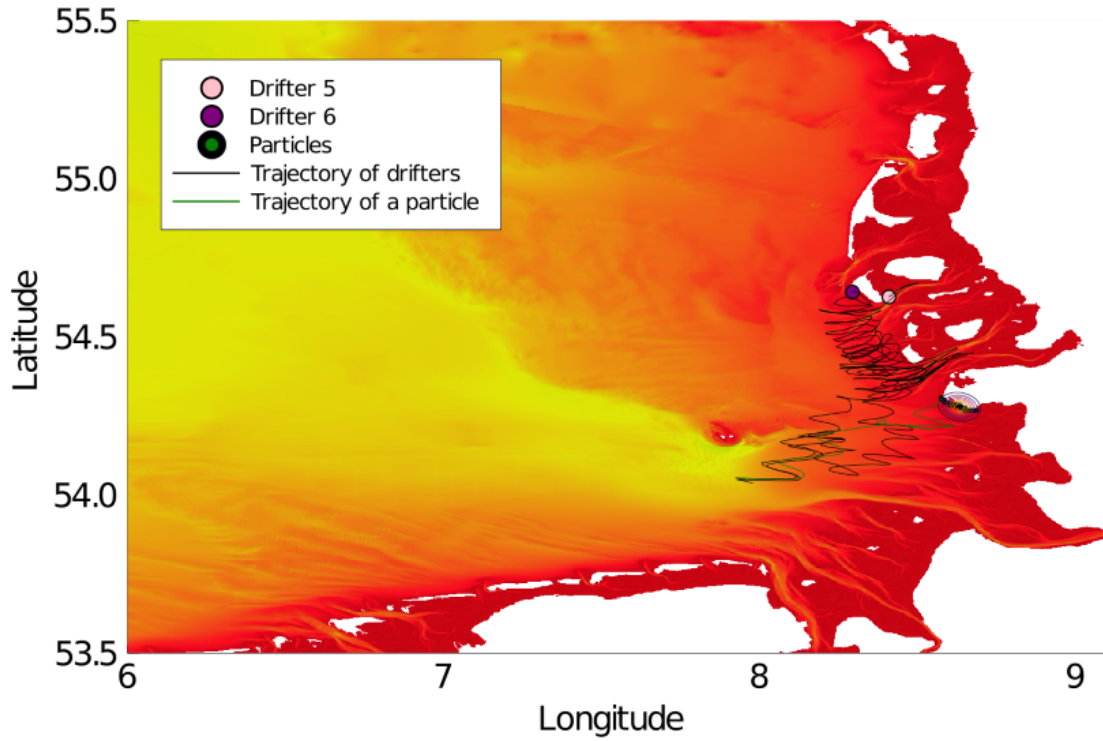


(a) Using the 3D velocity field.

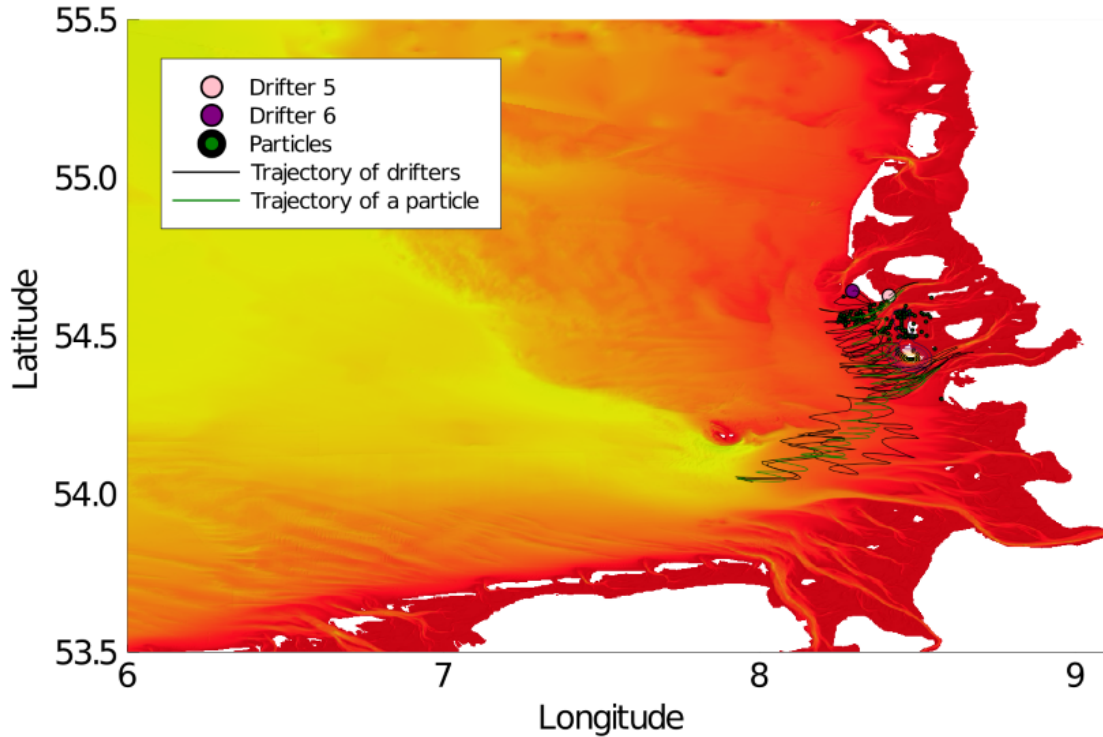


(b) Using the 2D velocity field.

Figure 12: Simulations of particles at time 2017-10-23T07:53, 300 particles initially at position of drifter 5, and 300 at the position of drifter 6. For the particle velocity, eq. 5 is used where $u_s = u_{s,jonswap}$, the Stokes drift estimated using the JONSWAP spectrum, eq 8.

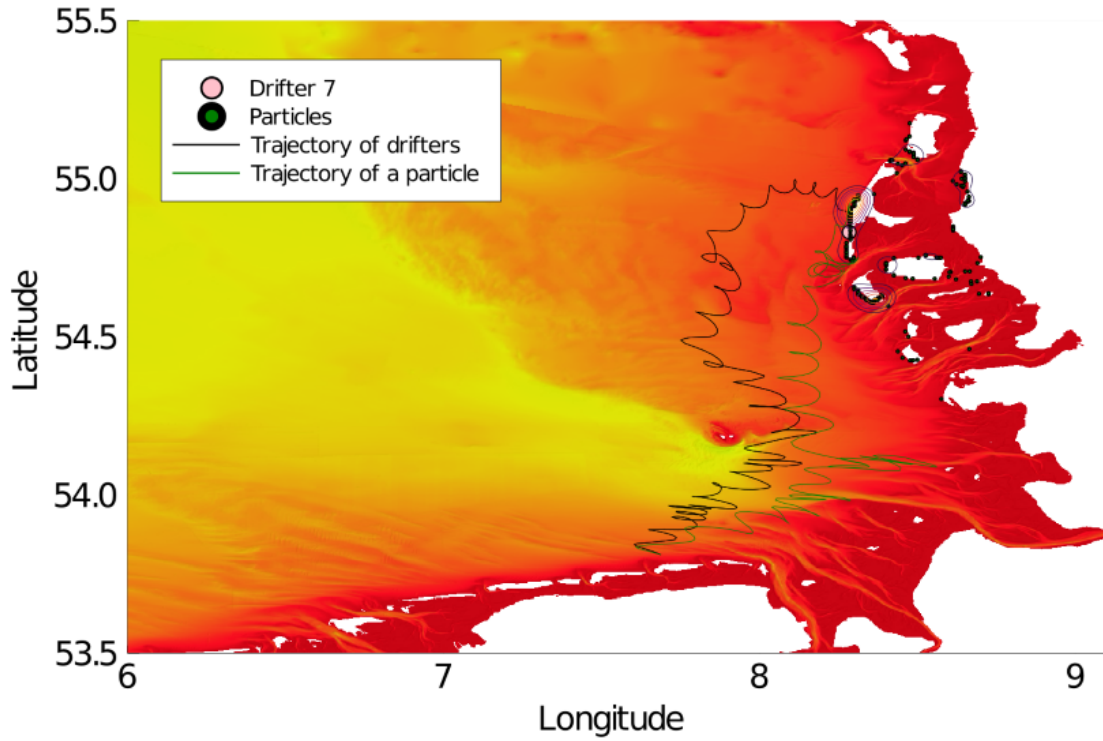


(a) Using the 3D velocity field.

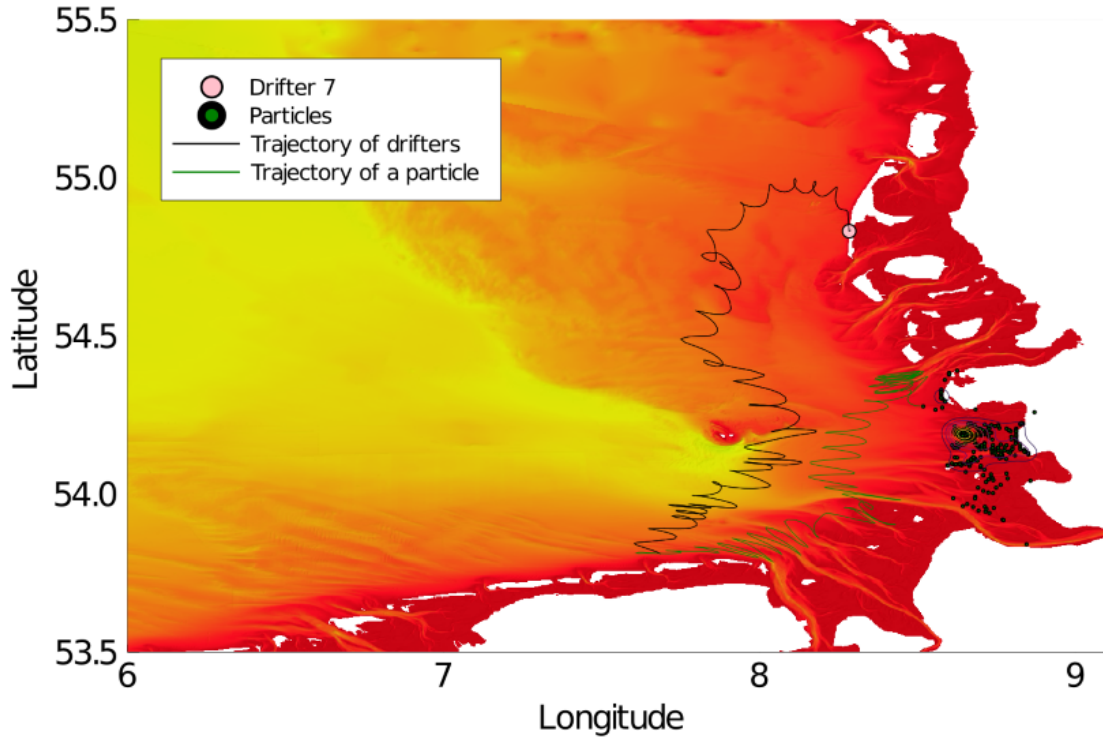


(b) Using the 2D velocity field.

Figure 13: Simulations of particles at time 2017-10-23T07:53, 300 particles initially at position of drifter 5, and 300 at the position of drifter 6. For the particle velocity, eq. 5 is used where $u_s = 1.6\%u_a$, the Stokes drift estimated using the 1.6% wind estimation.

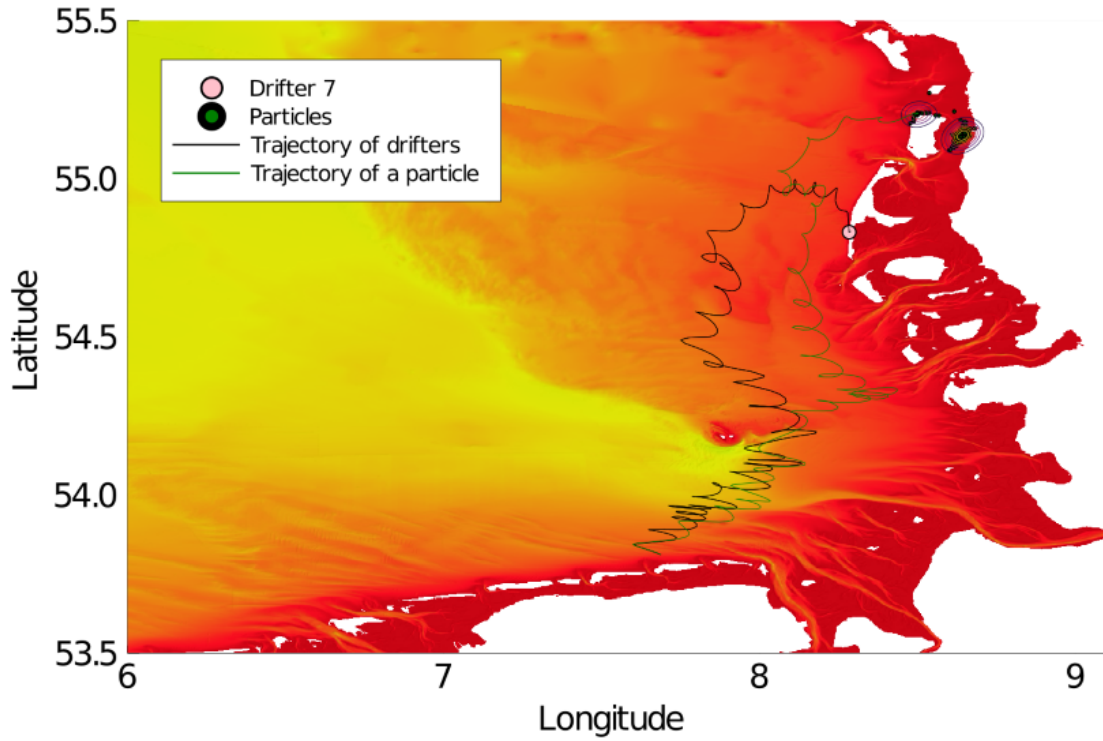


(a) Using the 3D velocity field.

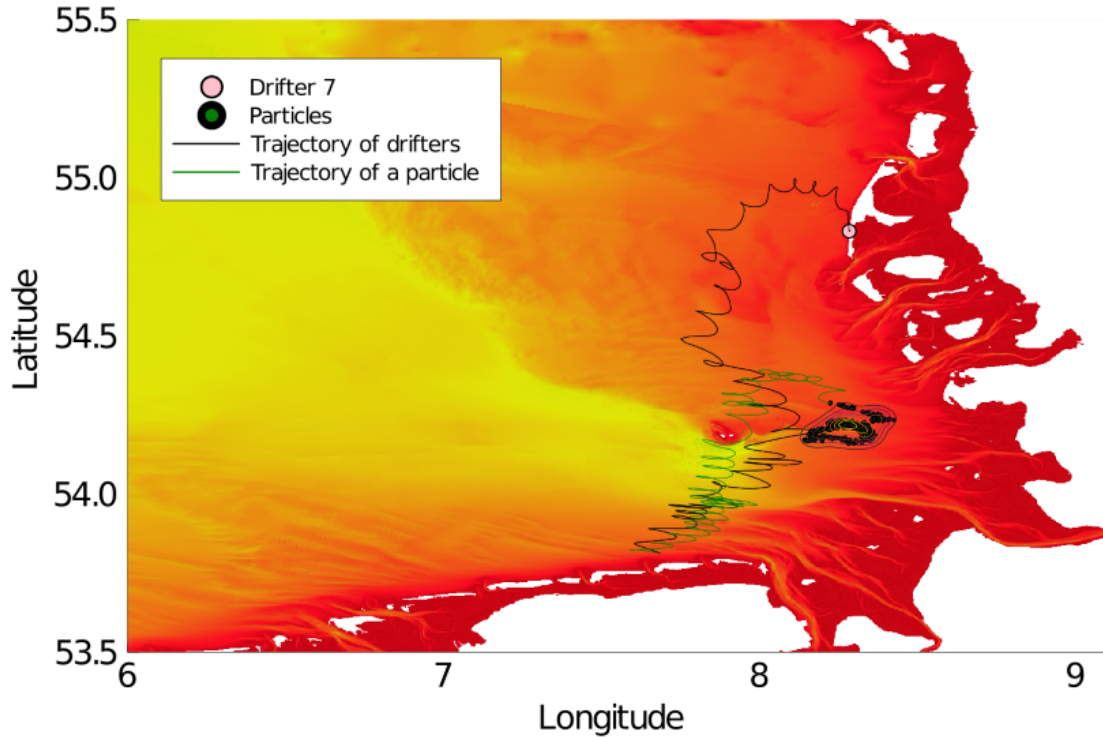


(b) Using the 2D velocity field.

Figure 14: Simulations of particles at time 2017-10-23T07:53, 300 particles initially at position of drifter 5, and 300 at the position of drifter 6. For the particle velocity, eq. 5 is used where $u_s = u_{s,jonswap}$, the Stokes drift estimated using the JONSWAP spectrum, eq 8.



(a) Using the 3D velocity field.



(b) Using the 2D velocity field.

Figure 15: Simulations of particles at time 2017-10-23T07:53, 300 particles initially at position of drifter 5, and 300 at the position of drifter 6. For the particle velocity, eq. 5 is used where $u_s = 1.6\%u_a$, the Stokes drift estimated using the 1.6% wind estimation.

4.3.3 Backwards simulation

For the backwards in time simulation, no the actual endtime of the drifters where used. Some drifters recorded their position until the shore was reach. Near the coast, the water velocity is inaccurate and the waterdepth small. To avoid these problem, the time 24 hours before the end of the timeseries is chosen and displayed in figure 16-22. Furthermore, as the drifter pairs from the previous sections have not similar end positions, results are displayed in separate figures.

It can be observed from these figures, that there are particles which have trajectories similar to the original drifter and origins of these drifter can be calculated. However, the spread of the particles is wider than the forwards direction, which makes predictions less accurate. Moreover, the results of this model are unreliable, as the quality of the results vary among each drifter.

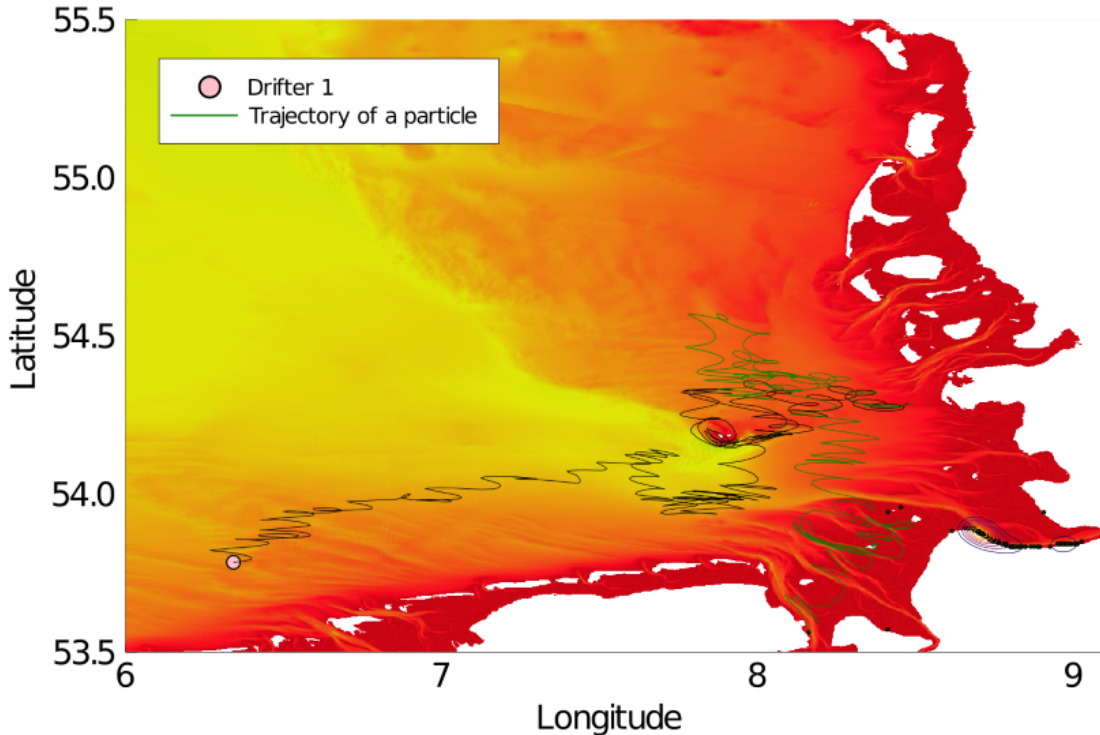


Figure 16: Backwards simulation for drifters 1, where the initial position is the end position of the drifter and the Itô SDE evolves backwards in time until the initial time of the drifter.

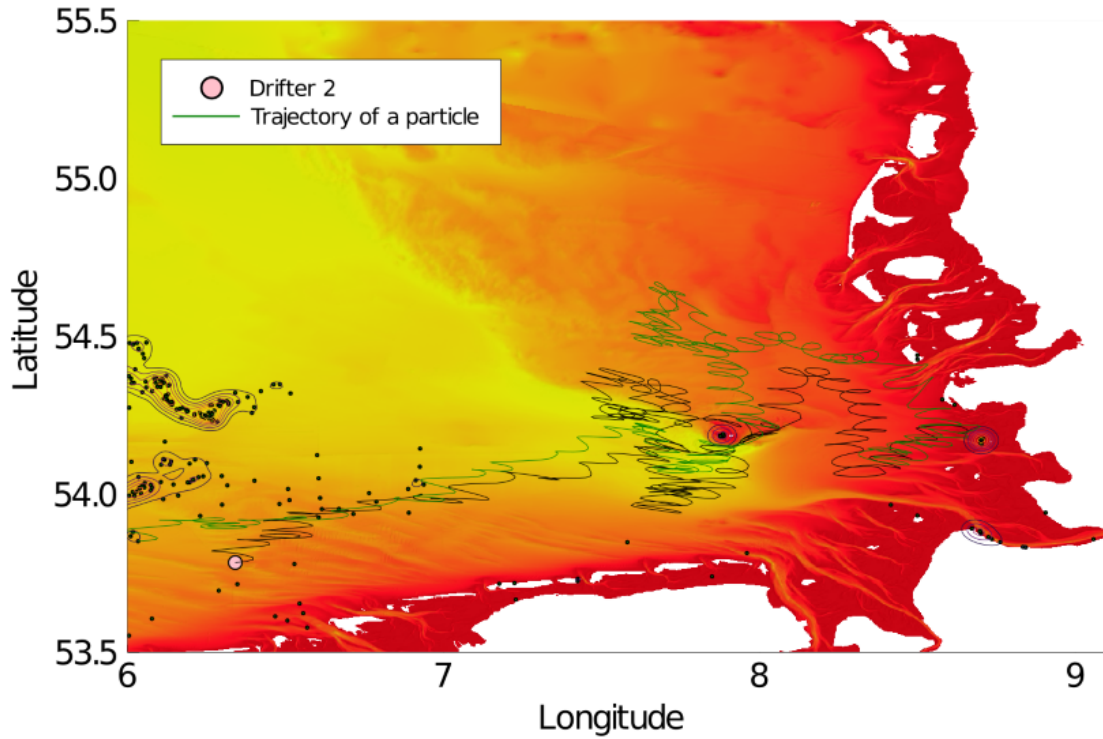


Figure 17: Backwards simulation for drifters 2, where the initial position is the end position of the drifter and the Itô SDE evolves backwards in time until the initial time of the drifter.

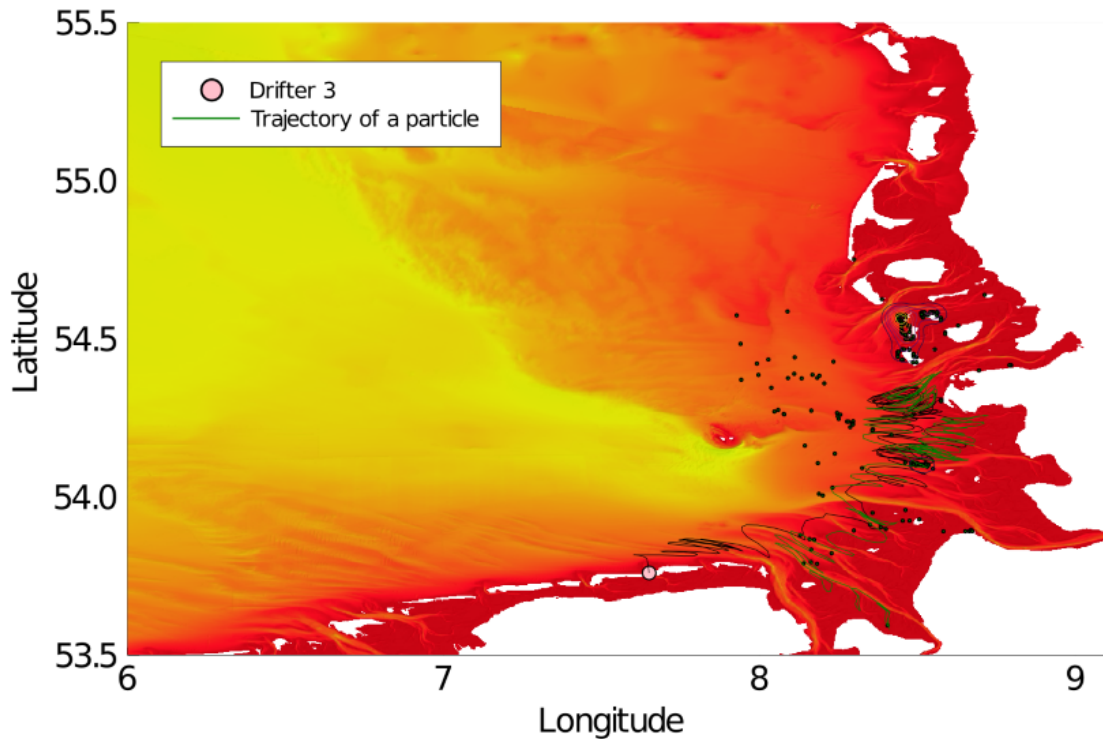


Figure 18: Backwards simulation for drifters 3, where the initial position is the end position of the drifter and the Itô SDE evolves backwards in time until the initial time of the drifter.

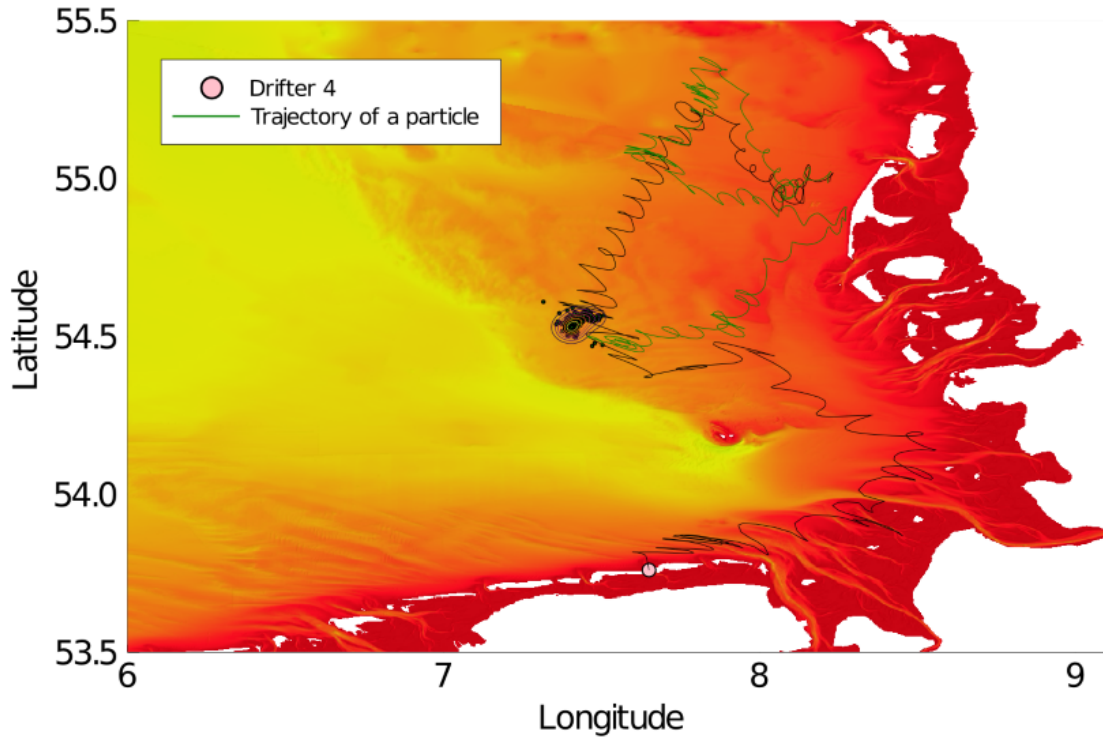


Figure 19: Backwards simulation for drifters 4, where the initial position is the end position of the drifter and the Itô SDE evolves backwards in time until the initial time of the drifter.

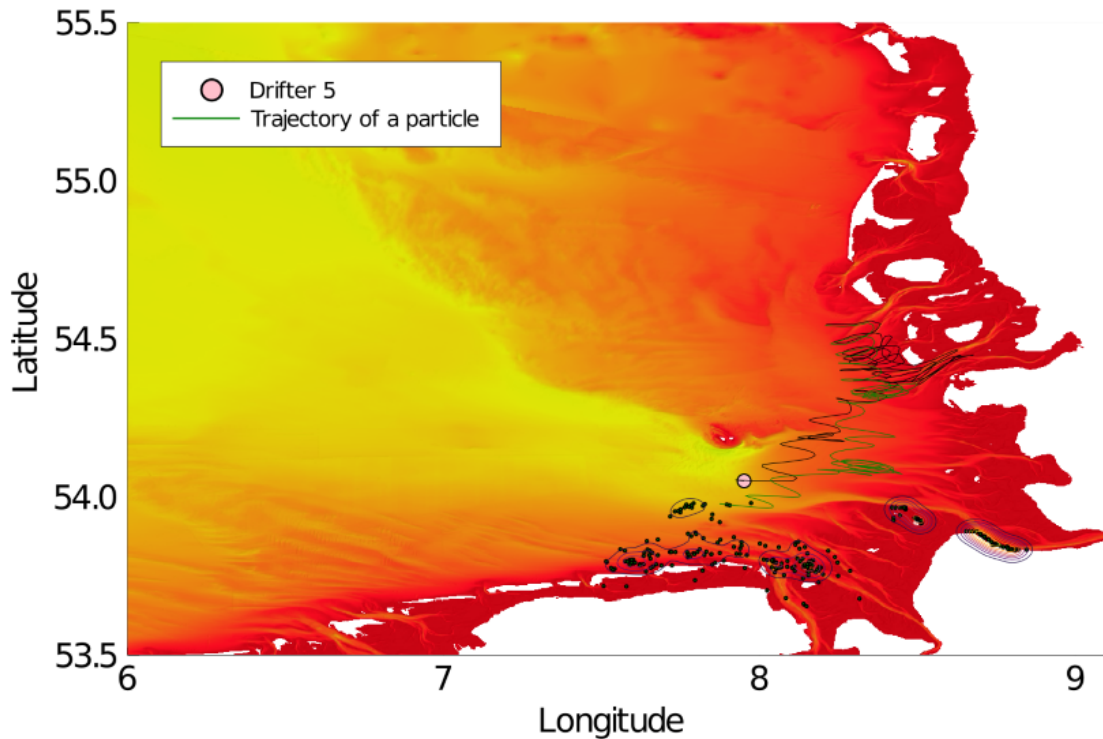


Figure 20: Backwards simulation for drifters 5, where the initial position is the end position of the drifter and the Itô SDE evolves backwards in time until the initial time of the drifter.

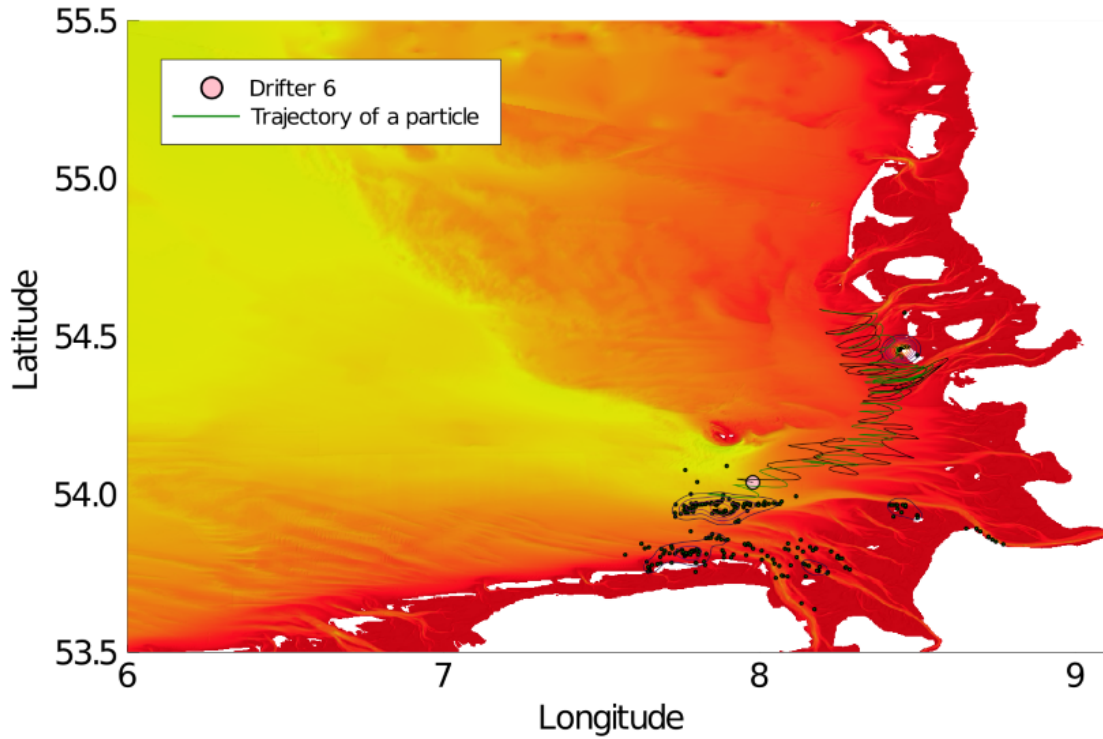


Figure 21: Backwards simulation for drifters 6, where the initial position is the end position of the drifter and the Itô SDE evolves backwards in time until the initial time of the drifter.

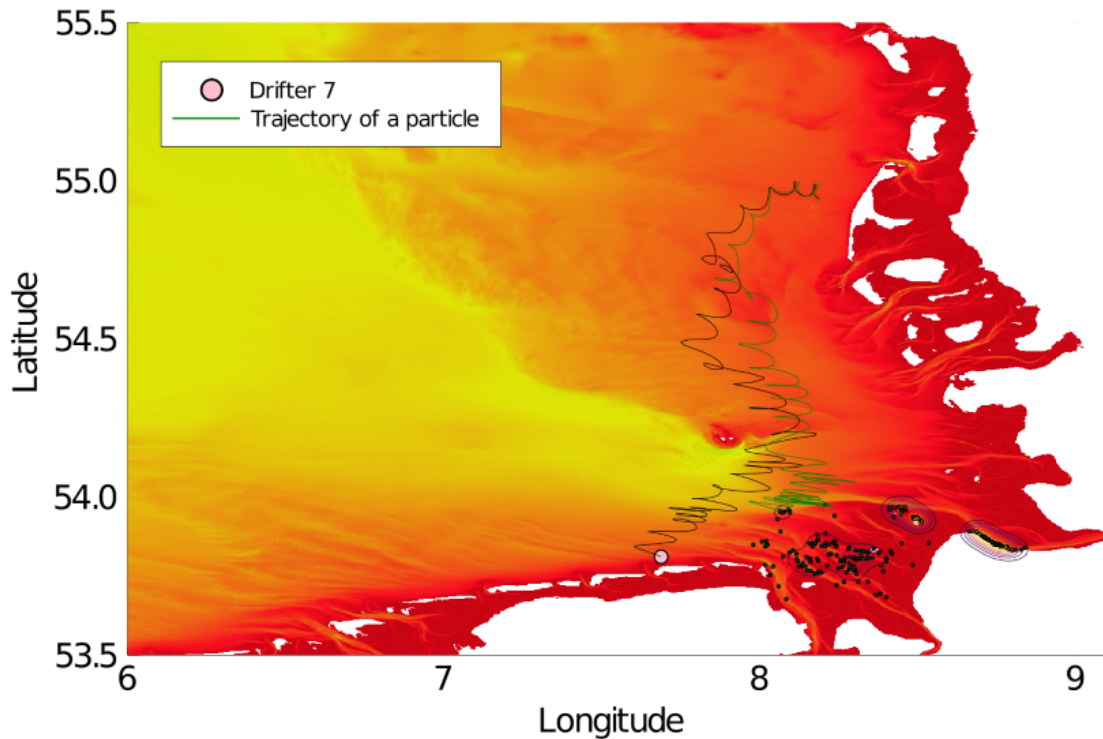


Figure 22: Backwards simulation for drifters 7, where the initial position is the end position of the drifter and the Itô SDE evolves backwards in time until the initial time of the drifter.

4.4 Lyapunov exponent

As drifters in the German Bight are studied in March and October of 2017, the finite time Lyapunov exponent of the 3D current is calculated in this period. As there is current data available from $t_0 = 2017-03-10T00:00$, this is taken as the initial time. The Lyapunov exponent calculations over 10 days is displayed in figure 23. A similar result can be obtained when calculating this for October, using $t_0 = 2017-10-08T00:00$.

The results are displayed in figure 23 and 24. Note that both periods similar have Lyapunov exponents.

It can be observed that the Lyapunov is close to zero for the majority of the sea, and the trajectories are neither converging nor diverging with the exception of a few spots. However, closer towards the coast, the German Bight and Helgoland, this number increases. This indicates that it gets increasingly more complicated to make long term predictions of the trajectory as it gets closer towards these areas. This is also indicated by figure 3, where the velocities are less predictable near the coastal area and the German Bight.

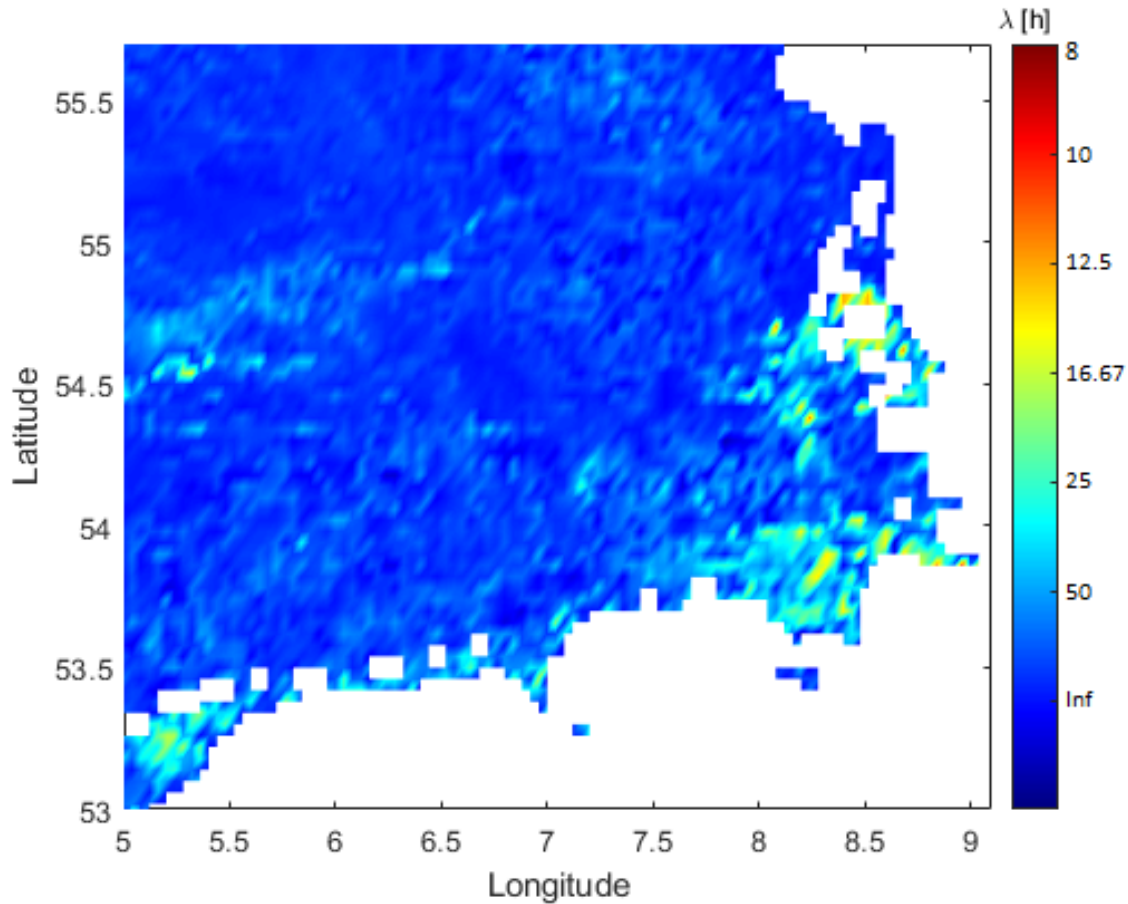


Figure 23: Lyapunov exponent $\lambda[\text{hour}^{-1}]$, displayed here as λ^{-1} , of the German Bight where $t = 10\text{days}$ and $t_0 = 2017-03-10T00:00$.

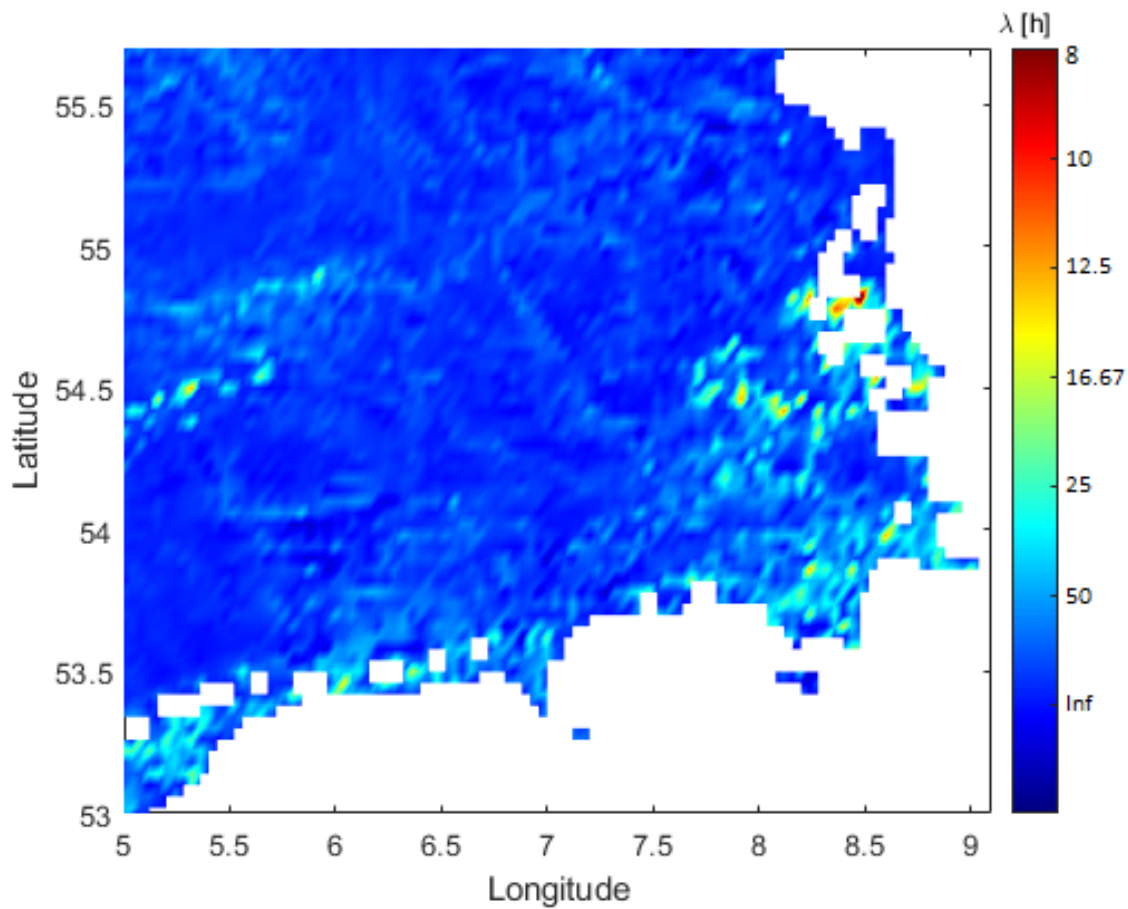


Figure 24: Lyapunov exponent λ [hour $^{-1}$], displayed here as λ^{-1} , of the German Bight where $t = 10$ days and $t_0 = 2017-10-08T00:00$.

5 Conclusion

The goal of this report was to verify whether a 3D water current model in combination with Stokes drift can better predict the trajectories of Lagrangian particles opposed to a 2D current model. In this case, the modeled trajectories are compared to the drifter position datasets from Meyerjürgens et al.[3].

From the results, it can be concluded that without the use of Stokes drift, the 3D velocity field improves the calculations of particle trajectories opposed to a 2D velocity field and can accurately estimate the drifter trajectories. There is a wide spread between particles trajectories, but this is comparable with distance of drifter pairs, initially close together. This is also indicated by the finite time Lyapunov exponent.

The decoupling of waves and addition of the Stokes drift does not result in better predictions. The accuracy of the Stokes drift estimations and the nonlinear effects in this area should be explored further before including this effect in further calculation. This could be done, by implementing the wave model directly into the water velocity calculations.

Furthermore, the trajectories diverges from the measured drifters near the island Helgoland. Investigating this area, starting with the bathymetry, and improving the velocity model near this area can provide better results.

6 Appendix

6.1 Deep water Stokes drift

Deriving a deep water Stokes drift approximation, we start with the original equation 25 as given in Kenton[7],

$$\begin{aligned} \mathbf{u}_s &= g \int_{-\infty}^{\infty} F(\mathbf{k}) \frac{\mathbf{k}}{\omega} \left[\frac{2k \cosh(2k(z+d))}{\sinh(2kd)} \right] d\mathbf{k} \\ &= g \int_0^{\infty} \int_{-\pi}^{\pi} F(k, \theta) \frac{2k^2 \hat{\mathbf{k}}(\theta)}{\omega} \left[\frac{\cosh(2k(z+d))}{\sinh(2kd)} \right] d\theta dk \\ &= g \int_0^{\infty} \int_{-\pi}^{\pi} F(k, \theta) \frac{2k^2 \hat{\mathbf{k}}(\theta)}{\omega} \left[\frac{\cosh(2kz)}{\tanh(2kd)} + \sinh(2kz) \right] d\theta dk \end{aligned} \quad (25)$$

To derive the equation, the dispersion relation for water waves is used[6];

$$\omega^2 = (2\pi f)^2 = gk \tanh(kd) \text{ and } \lambda = \frac{gT^2}{2\pi} \tanh\left(\frac{2\pi d}{\lambda}\right) \quad (26)$$

For deep water, where $\lambda \ll d$, we find $\tanh(kd) \rightarrow 1$ as $kd \rightarrow \infty$, which simplifies the dispersion relation as $k = \frac{4\pi^2 f^2}{g}$ and the resulting Stokes drift becomes

$$\mathbf{u}_s = g \int_0^{\infty} \int_{-\pi}^{\pi} F(k, \theta) \frac{2k^2 \hat{\mathbf{k}}(\theta)}{\omega} [\cosh(2kz) + \sinh(2kz)] d\theta dk \quad (27)$$

$$= g \int_0^{\infty} \int_{-\pi}^{\pi} F(k, \theta) \frac{2k^2 \hat{\mathbf{k}}(\theta)}{\omega} e^{2kz} dd\theta \quad (28)$$

$$= \frac{16\pi^3}{g} \int_0^{\infty} \int_{-\pi}^{\pi} (\cos \theta, \sin \theta, 0) f^3 F_{f\theta}(f, \theta) e^{\frac{8\pi^2 f^2 z}{g}} d\theta df. \quad (29)$$

Often, the wave spectrum is split[8] such that $\int_{-\pi}^{\pi} \phi(f, \theta) d\theta = 1$ and the stokes drift becomes

$$\mathbf{u}_s = \frac{16\pi^3}{g} \int_0^{\infty} \int_{-\pi}^{\pi} (\cos \theta, \sin \theta, 0) f^3 F_f(f) \phi(f, \theta) e^{\frac{8\pi^2 f^2 z}{g}} d\theta df \quad (30)$$

$$= \frac{16\pi^3}{g} \int_0^{\infty} \mathbf{H}(f) f^3 F_f(f) e^{\frac{8\pi^2 f^2 z}{g}} df \quad (31)$$

If an unidirectional wave field is evaluated, where the wave spectrum is separable, $\mathbf{H}(f)$ simply represents the wave direction. However, if this is not the case, wave energy is loss in other direction then the dominant wave direction, and a $\mathbf{H}(f)$ represent the loss of Stokes drift due to this effect.

With this, the magnitude of the Stokes drift at the surface $z = 0$ becomes the third moment of the wave spectral density[8], resulting in

$$u_s|_{z=0} = \frac{16\pi^3}{g} \int_0^\infty f^3 F_f(f) e^{\frac{8\pi^2 f^2 z}{g}} df \quad (32)$$

$$= \frac{16\pi^3}{g} \int_0^\infty f^3 F_f(f) df \quad (33)$$

$$= \frac{\pi^3 H_{m0}^2}{g T_3^3} \quad (34)$$

where H_{m0} and T_3 represent the significant wave height and the third period respectively.

6.2 Validation deep water approximation

The approximation of the Stokes drift from the previous section 6.1, is only valid for deep water wave, $\lambda \ll d$ and close to the surface, $z \rightarrow 0$. However, as the drifters and simulations in this project reside in the coastal area of the North Sea, this approximation might not be valid.

To validate whether this approximation hold, the JONSWAP spectrum[9] is used for the wave spectral density;

$$F(f) = \alpha g^2 (2\pi)^{-4} f^{-5} \exp\left(-\frac{5}{4} \left(\frac{f}{f_p}\right)^{-4}\right) \gamma^{\exp\left(\frac{-(f-f_p)^2}{2\sigma^2 f_p^2}\right)} \quad (35)$$

$$\sigma = \begin{cases} 0.07 & \text{if } f \leq f_p \\ 0.09 & \text{if } f > f_p \end{cases}$$

$$\alpha = 5.3 \cdot 10^{-3}$$

$$\gamma = 3.3$$

where g is the gravitational constant and f_p the peak frequency.

For an arbitrary water depth, the dispersion relation 26 does not simplify, resulting in an implicit expression for k . Therefore, the Stokes drift eq.25 will not be solved analytically, but numerically. For this test case, an unidirectional wave field is used, resulting in equation 32 for the deep water equation and for arbitrary waterdepth;

$$u_s = g \int_0^\infty F(k) \frac{2k^2}{\omega} \left[\frac{\cosh(2k(z+d))}{\sinh(2kd)} \right] dk. \quad (36)$$

The results of the numerical solution for both equations 32 and 36 are displayed in figure 25. Note that the magnitude of the Stokes drift is increasing as the water becomes shallow. However, in reality, this is not necessarily the case.

The equation for the Stokes drift is valid for a unidirectional wave field. However, as the waves get closer to the shore, because of refraction, the waves bend towards the shore, resulting in energy loss in the dominant wave direction as the wave field is not unidirectional anymore. Also, other coastal effect such as shoaling and undertow the Stokes drift will not necessarily increase.

6.3 Simulations without wind

In figure 26-29, results are displayed where not Stokes drift $u_s = 0$ and no drag as a result of the wind are including, thus $u_p = u_{water}$. As the figure indicate, these results are similar to the results from section 4.3.1. This is explained by the fact that $\frac{k_w}{k_w+k_a} \approx 0.998$, indicating that the drifters are mainly influenced by the water. The drifters therefore give a accurate representation of the Lagrangian properties of the water in the German Bight.

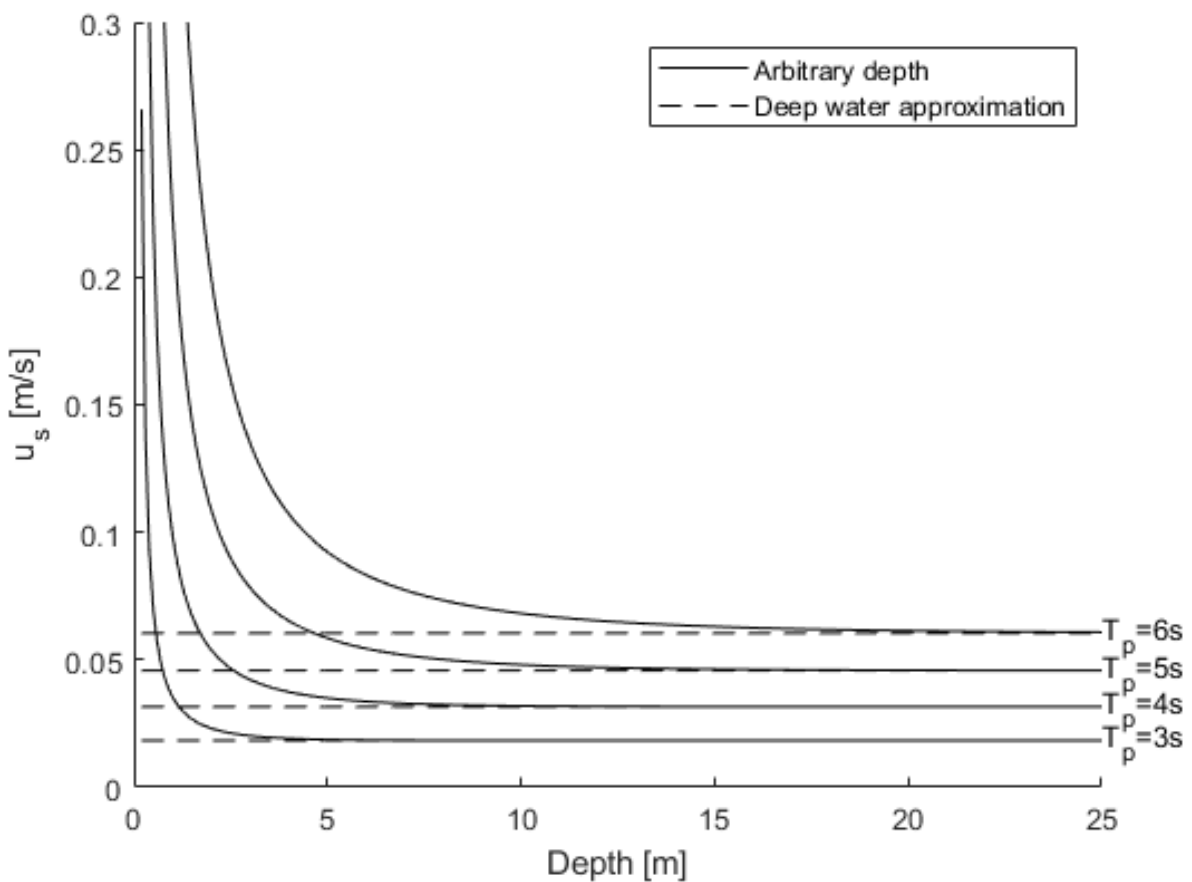
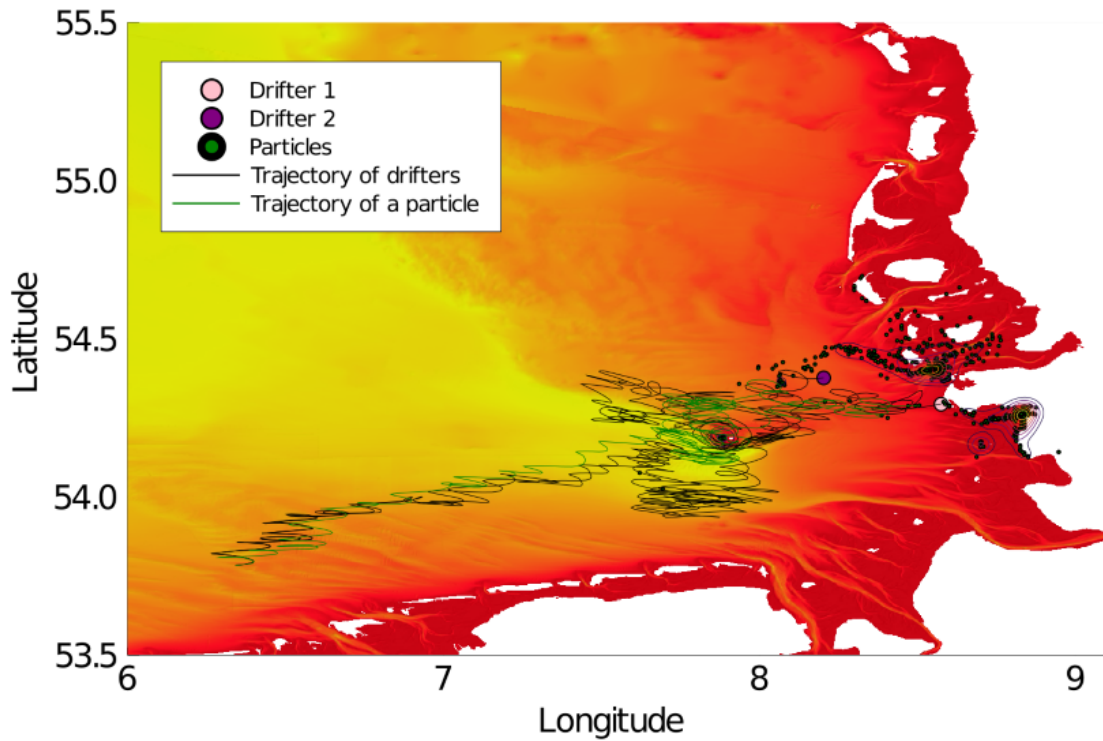
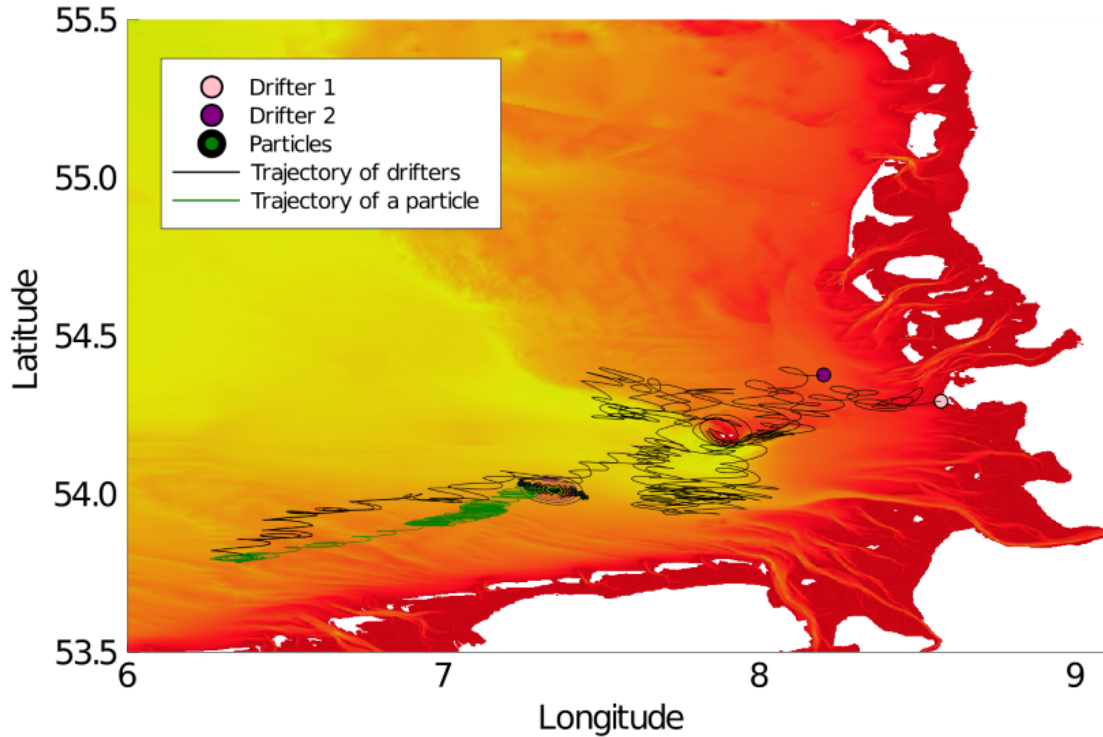


Figure 25: Numerical solution for the Stokes drift for various peak periods T_p , were $T_p = \frac{1}{f_p}$ using the eq.36 for arbitrary depth and eq.32 for the deep water approximation using $z = 0.25m$.

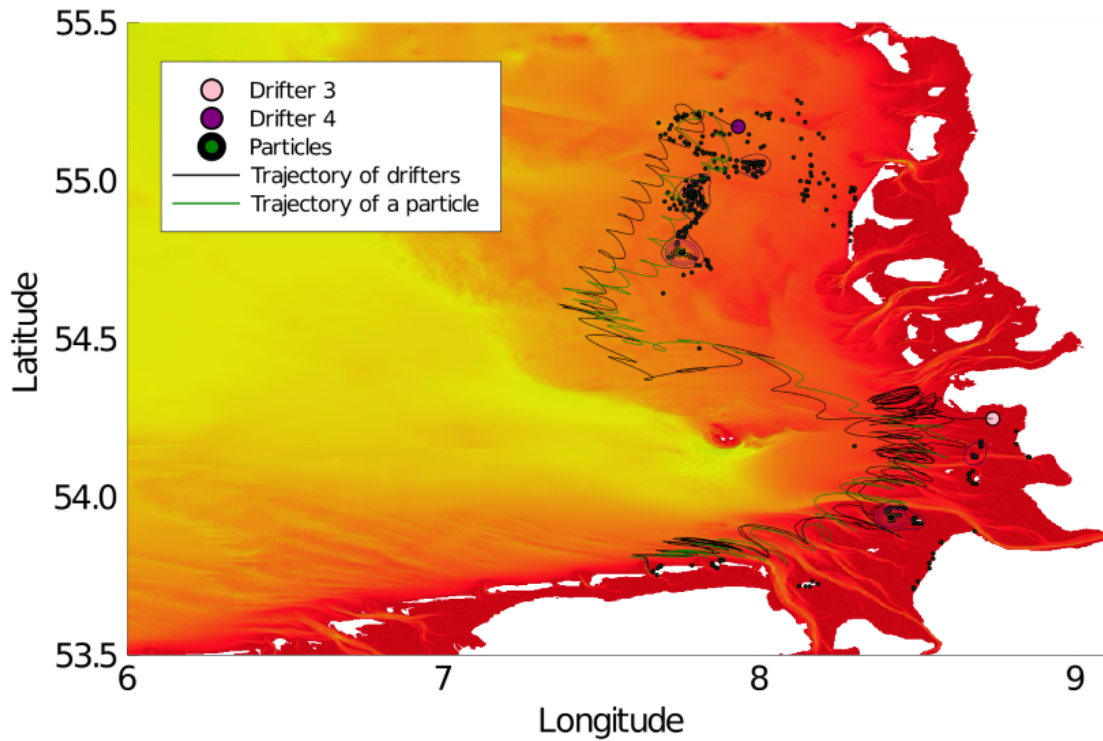


(a) Using the 3D velocity field.

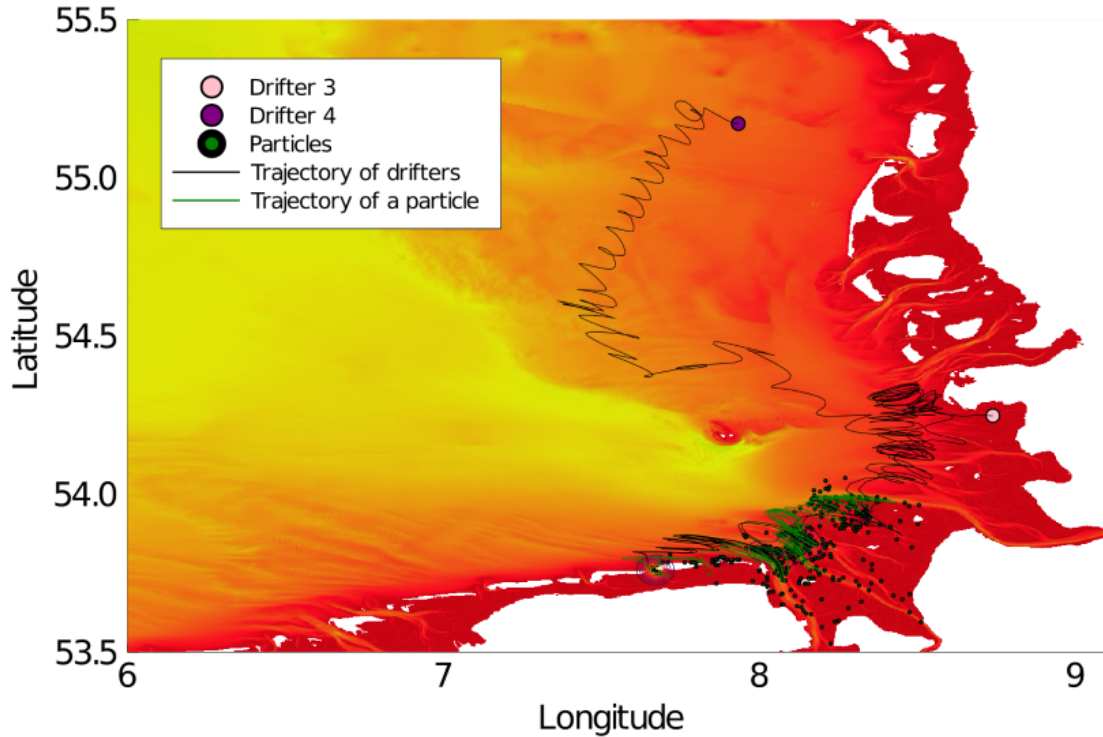


(b) Using the 2D velocity field.

Figure 26: Simulations of particles at time 2017-04-15T15:10, 300 particles initially at position of drifter 1, and 300 at the position of drifter 2. For the particle velocity, $u_p = u_{water}$, thus no wind drag and no Stokes drift.

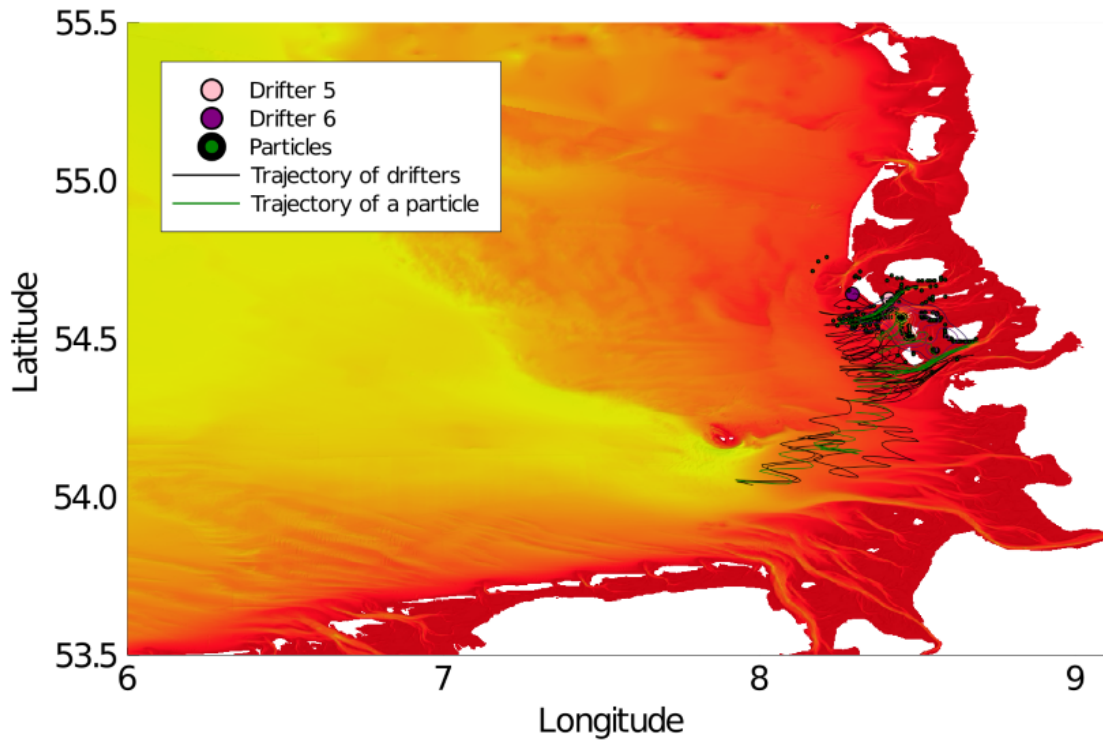


(a) Using the 3D velocity field.

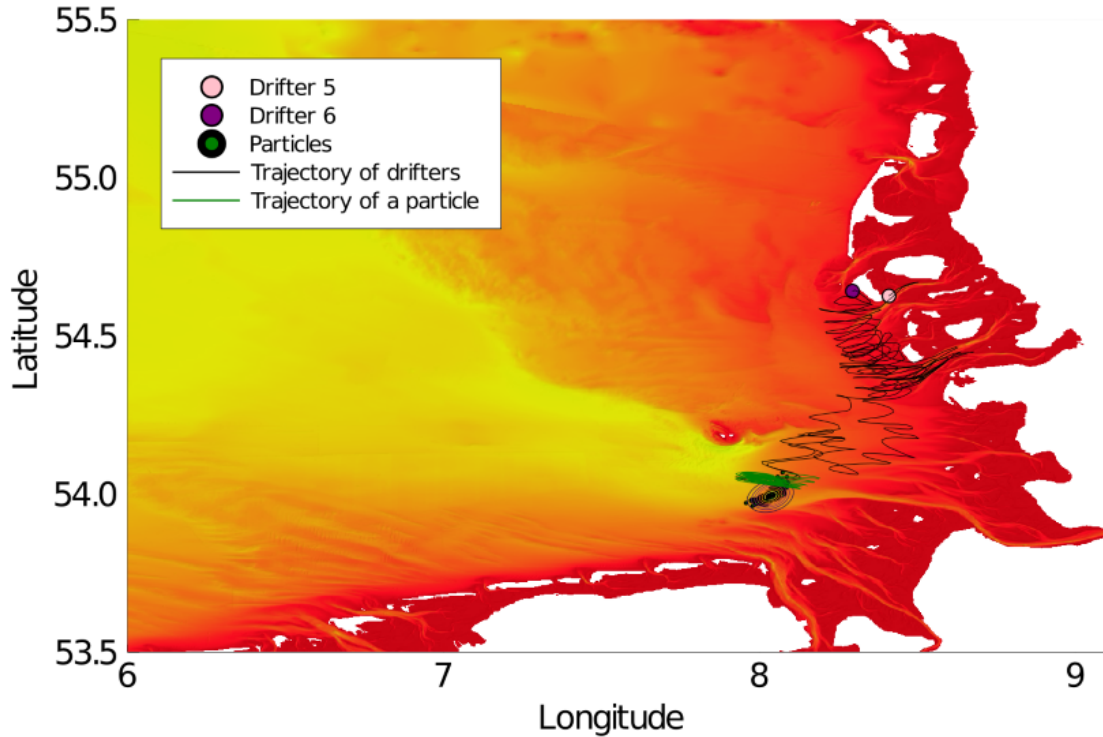


(b) Using the 2D velocity field.

Figure 27: Simulations of particles at time 2017-04-05T20:57, 300 particles initially at position of drifter 3, and 300 at the position of drifter 4. For the particle velocity, $u_p = u_{water}$, thus no wind drag and no Stokes drift.

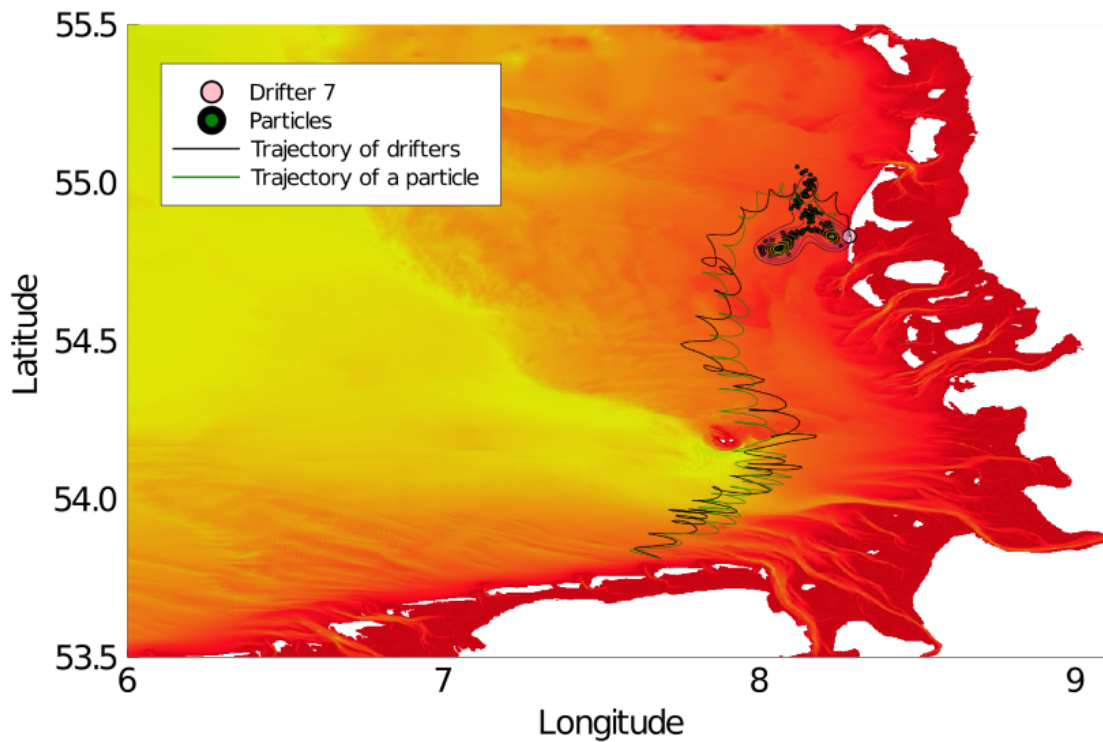


(a) Using the 3D velocity field.

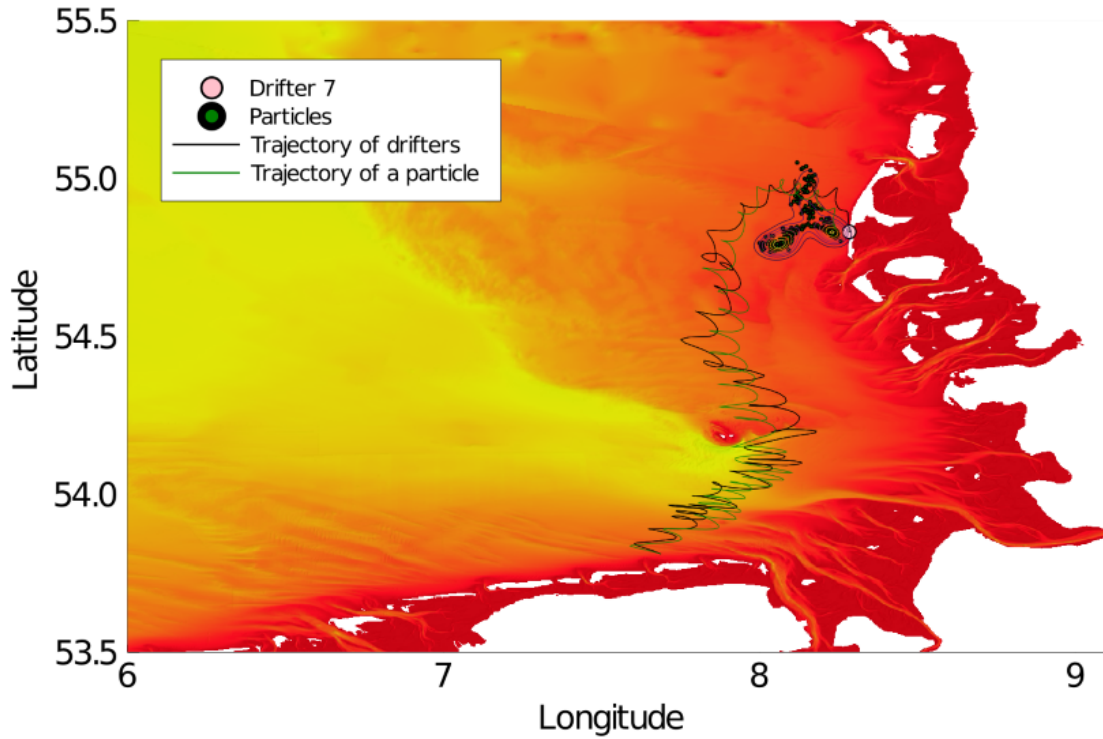


(b) Using the 2D velocity field.

Figure 28: Simulations of particles at time 2017-10-23T07:53, 300 particles initially at position of drifter 5, and 300 at the position of drifter 6. For the particle velocity, $u_p = u_{water}$, thus no wind drag and no Stokes drift.



(a) Using the 3D velocity field.



(b) Using the 2D velocity field.

Figure 29: Simulations of particles at time 2017-10-27T12:58, 300 particles initially at position of drifter 7. For the particle velocity, $u_p = u_{water}$, thus no with drag and no Stokes drift.

6.4 Backwards finite time Lyapunov exponent

In section 3.6, the finite time Lyapunov exponent is described. Here, the assumption was made that time t was positive, thus from an initial time t_0 , eq. 22 is in the forwards direction. However, if instead of going forward, the backwards formulation is used, meaning t represents a time before the initial time, the backwards ftle can be estimated. The results are displayed in fig. 30 and 31. Note that these results are similar as the forward ftle from fig. 23 and 31.

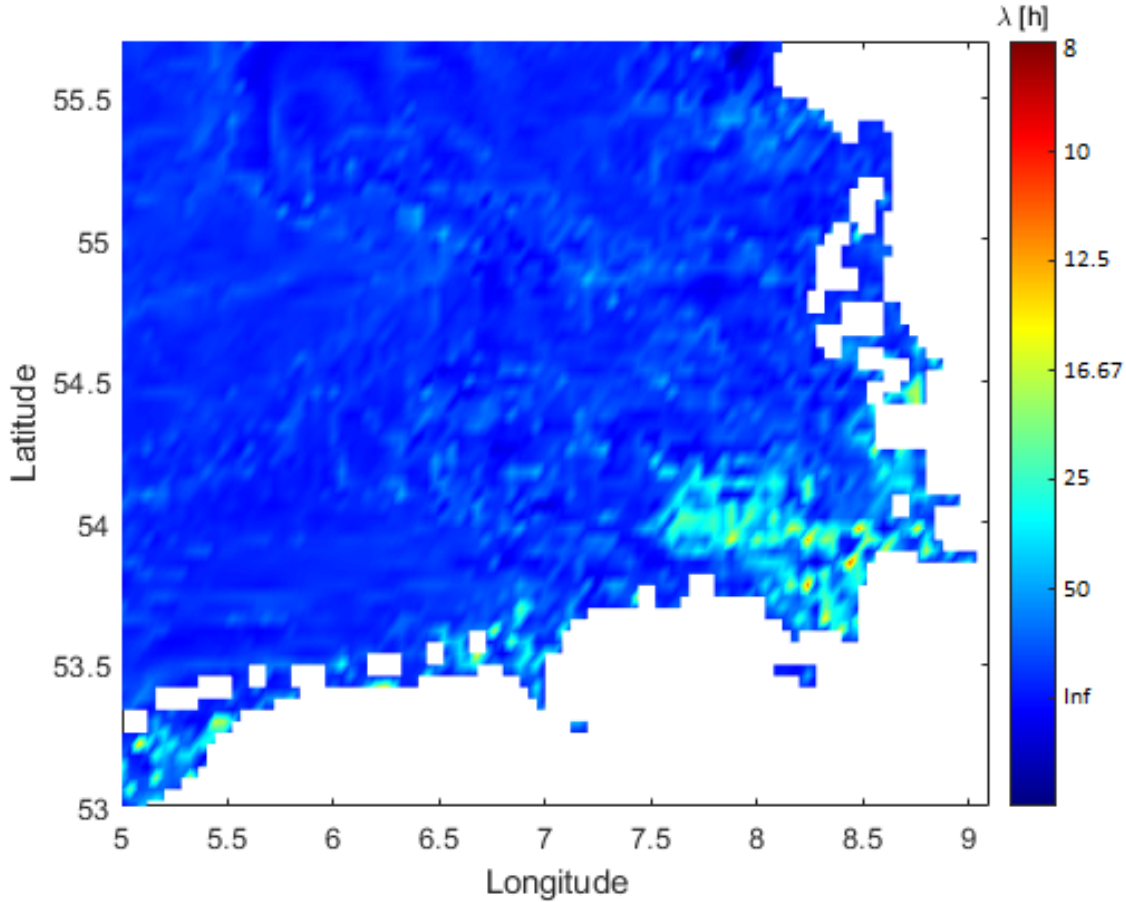


Figure 30: Lyapunov exponent $\lambda[\text{hour}^{-1}]$, displayed here as λ^{-1} , of the German Bight where $t = 10\text{days}$ and $t_0 = 2017-04-22T00:00:00$.

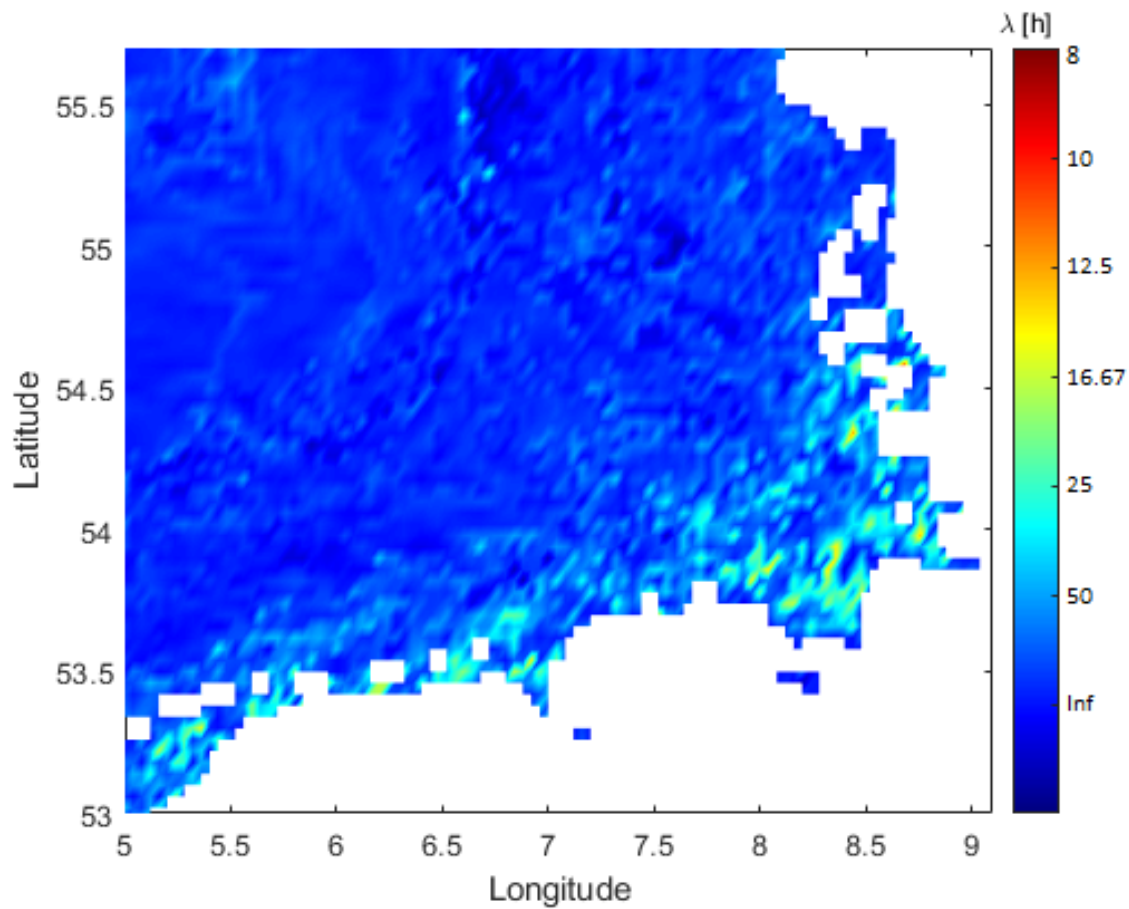


Figure 31: Lyapunov exponent λ [hour $^{-1}$], displayed here as λ^{-1} , of the German Bight where $t = 10$ days and $t_0 = 2018-10-29T00:00:00$.

References

- [1] C. Ioakeimidis, F. Galgani, and G. Papatheodorou, *Occurrence of Marine Litter in the Marine Environment: A World Panorama of Floating and Seafloor Plastics*, pp. 93–120. Cham: Springer International Publishing, 2019.
- [2] B. D. Hardesty, J. Harari, A. Isobe, L. Lebreton, N. Maximenko, J. Potemra, E. van Sebille, A. D. Vethaak, and C. Wilcox, “Using numerical model simulations to improve the understanding of microplastic distribution and pathways in the marine environment,” *Frontiers in Marine Science*, vol. 4, p. 30, 2017.
- [3] J. Meyerjürgens, T. H. Badewien, S. P. Garaba, J.-O. Wolff, and O. Zielinski, “A state-of-the-art compact surface drifter reveals pathways of floating marine litter in the german bight,” *Frontiers in Marine Science*, vol. 6, p. 58, 2019.
- [4] E. Ooms, “Implementation of stokes drift into a particle model.” Internship Deltas, Environmental Hydrodynamics and Forecasting, and TU Delft, 2 2020.
- [5] E. Anderson, A. Odulo, and M. Spaulding, “Modeling of leeway drift,” *U.S. Coast Guard Research and Development Center*, p. 58, 09 1998.
- [6] L. H. Holthuijsen, *Waves in Oceanic and Coastal Waters*. Cambridge University Press, 2007.
- [7] K. E. Kenyon, “Stokes drift for random gravity waves,” *Journal of Geophysical Research (1896-1977)*, vol. 74, no. 28, pp. 6991–6994, 1969.
- [8] A. Webb and B. Fox-Kemper, “Wave spectral moments and stokes drift estimation,” *Ocean Modelling*, vol. 40, no. 3, pp. 273 – 288, 2011.
- [9] K. Hasselmann, T. Barnett, E. Bouws, H. Carlson, D. Cartwright, K. Enke, J. Ewing, H. Gienapp, D. Hasselmann, P. Kruseman, A. Meerburg, P. Muller, D. Olbers, K. Richter, W. Sell, and H. Walden, “Measurements of wind-wave growth and swell decay during the joint north sea wave project (jonswap),” *Deut. Hydrogr. Z.*, vol. 8, pp. 1–95, 01 1973.
- [10] E. van Sebille, S. M. Griffies, R. Abernathey, T. P. Adams, P. Berloff, A. Biastoch, B. Blanke, E. P. Chassignet, Y. Cheng, C. J. Cotter, E. Deleersnijder, K. Döös, H. F. Drake, S. Drijfhout, S. F. Gary, A. W. Heemink, J. Kjellsson, I. M. Koszalka, M. Lange, C. Lique, G. A. MacGilchrist, R. Marsh, C. G. M. Adamej, R. McAdam, F. Nencioli, C. B. Paris, M. D. Piggott, J. A. Polton, S. Rühs, S. H. Shah, M. D. Thomas, J. Wang, P. J. Wolfram, L. Zanna, and J. D. Zika, “Lagrangian ocean analysis: Fundamentals and practices,” *Ocean Modelling*, vol. 121, pp. 49 – 75, 2018.
- [11] J. M. Toole, *Turbulent Mixing in the Ocean*, pp. 171–190. Dordrecht: Springer Netherlands, 1998.
- [12] A. Soloviev and R. Lukas, *The Near-Surface Layer of the Ocean*, vol. 31. Springer, 2006.
- [13] J. Blazek, “Chapter 7 - turbulence modeling,” in *Computational Fluid Dynamics: Principles and Applications (Third Edition)* (J. Blazek, ed.), pp. 213 – 252, Oxford: Butterworth-Heinemann, third edition ed., 2015.
- [14] E. R. Abraham and M. M. Bowen, “Chaotic stirring by a mesoscale surface-ocean flow,” *Chaos: An Interdisciplinary Journal of Nonlinear Science*, vol. 12, no. 2, pp. 373–381, 2002.
- [15] X. Tang and A. Boozer, “Finite time lyapunov exponent and advection-diffusion equation,” *Physica D: Nonlinear Phenomena*, vol. 95, no. 3, pp. 283 – 305, 1996.
- [16] J. Meyerjürgens, T. H. Badewien, O. Zielinski, A. Braun, and M. Butter, “Track of GPS-Drifter North_Sea_Drifter1 in the German Bight, Southern North Sea,” 2019.
- [17] J. Meyerjürgens, T. H. Badewien, O. Zielinski, A. Braun, and M. Butter, “Track of GPS-Drifter North_Sea_Drifter2 in the German Bight, Southern North Sea,” 2019.

- [18] J. Meyerjürgens, T. H. Badewien, O. Zielinski, A. Braun, and M. Butter, “Track of GPS-Drifter North_Sea_Drifter3 in the German Bight, Southern North Sea,” 2019.
- [19] J. Meyerjürgens, T. H. Badewien, O. Zielinski, A. Braun, and M. Butter, “Track of GPS-Drifter North_Sea_Drifter4 in the German Bight, Southern North Sea,” 2019.
- [20] J. Meyerjürgens, T. H. Badewien, O. Zielinski, A. Braun, and M. Butter, “Track of GPS-Drifter HE498/10-3 (North_Sea_Drifter5) in the German Bight, Southern North Sea,” 2019.
- [21] J. Meyerjürgens, T. H. Badewien, O. Zielinski, A. Braun, and M. Butter, “Track of GPS-Drifter North_Sea_Drifter6 in the German Bight, Southern North Sea,” 2019.
- [22] J. Meyerjürgens, T. H. Badewien, O. Zielinski, A. Braun, and M. Butter, “Track of GPS-Drifter North_Sea_Drifter7 in the German Bight, Southern North Sea,” 2019.
- [23] <https://ows.emodnet-bathymetry.eu/>.
- [24] C. Chafin, “The absence of stokes drift in waves,” 01 2016.